

Inferring aircraft icing from numerical weather prediction (NWP) model outputs

Luís António Gonçalves Rodrigues

Thesis to obtain the Master of Science Degree in

Aerospace Engineering

Supervisors: Prof. Pedro da Graça Tavares Álvares Serrão
Doutora Margarida Sena Belo Santos Pereira

Examination Committee

Chairperson: Prof. Paulo Jorge Coelho Ramalho Oliveira
Supervisor: Doutora Margarida Sena Belo Santos Pereira
Member of the Committee: Prof. David João da Silva Carvalho

July 2022

Dedicated to my niece and god-daughter Margarida.

Declaração

Declaro que o presente documento é um trabalho original da minha autoria e que cumpre todos os requisitos do Código de Conduta e Boas Práticas da Universidade de Lisboa.

Declaration

I declare that this document is an original work of my own authorship and that it fulfills all the requirements of the Code of Conduct and Good Practices of the Universidade de Lisboa.

Acknowledgments

Firstly, I would like to express my gratitude to my dissertation supervisors, Dr. Margarida Belo-Pereira and Prof. Pedro Serrão, for all their shared knowledge, guidance and support throughout this intense journey. It was a privilege to work with such kind, thoughtful and wise persons.

I would also like to thank my parents for the support during all these years. Without them, this journey would not be possible. To my brother: there are not enough words to thank you for the constant support, the patience, the advices, and for always being with me trough the highs and the lows. To my sister: thank you for always being there for me and for giving me the most beautiful niece I have ever seen. There is no ocean capable of keeping us apart.

To my close friends: thank you for your patience, for being there for me whenever I need, for the long conversations, and for keeping me motivated.

Lastly, I could not forget to mention the AeroTéc student group and the UAV-ART project for all experiences and memories, for the friendships, the team spirit, and all the skills and knowledge acquired during the last few years. Thank you for the opportunity to grow on a technical and, above all, personal level.

Resumo

A formação de gelo nas aeronaves representa uma grande ameaça para a aviação em geral. A acumulação de gelo nas superfícies das aeronaves, especialmente asas e cauda, pode levar a uma diminuição da sustentação, aumento do arrasto, perda de eficácia do controlo, e degradação geral do desempenho. Esta acumulação de gelo ocorre devido à presença de gotículas de água líquida a temperaturas negativas. Por este motivo, o desenvolvimento e melhoria dos algoritmos capazes de prever as condições favoráveis à formação de gelo são de grande importância.

Esta dissertação visa aumentar os conhecimentos sobre o ambiente propício à formação de gelo na região da Europa Ocidental. Para o efeito, foram analisados 27 relatos de pilotos (PIREPs) de eventos de formação de gelo (19 eventos moderados e 8 eventos severos). Estes dados são comparados com as previsões de variáveis atmosféricas relevantes correspondentes feitas por um modelo de Previsão Numérica do Tempo (PNT). Este conhecimento é útil para melhorar os algoritmos utilizados para este fim. Estes algoritmos usam funções de associação, que combinam várias variáveis previstas pelos modelos de PNT, para prever a formação de gelo nas aeronaves. Além disso, um novo algoritmo é comparado com duas outras alternativas: uma que está atualmente operacional em Portugal, desenvolvida pelo Instituto Português do Mar e da Atmosfera (IPMA), e a outra implementada no Reino Unido. Esta comparação é feita usando tabelas de contingência construídas para os três algoritmos para limiares específicos, e a respetiva avaliação objetiva.

Palavras-chave: Formação de gelo nas aeronaves, algoritmo baseado em PNT, funções de associação, PIREP, tabelas de contingência, verificação objetiva

Abstract

Aircraft icing poses a great threat to aviation in general. Ice accumulation on aircraft surfaces, especially wings and tail, can lead to a decrease in lift, increase in drag, loss of control effectiveness, and overall performance degradation. This ice accumulation occurs due to the presence of liquid water droplets at sub-freezing temperatures. For this reason, the development and improvement of algorithms capable of forecasting icing conditions are of great importance.

This dissertation aims at increasing the knowledge about the aircraft icing environment in the Western European region. For that purpose, 27 Pilot Reports (PIREPs) of icing events (19 moderate events and 8 severe events) were analyzed. These data are compared with the corresponding forecasts of important atmospheric variables from a Numerical Weather Prediction (NWP) model output. This knowledge is helpful to improve the icing algorithms based on membership functions that use NWP model outputs to predict aircraft icing. Moreover, one new algorithm is compared with two other alternatives: one that is currently operational in Portugal, developed by IPMA, and the other implemented by the Met Office in the UK. This comparison is made using contingency tables derived from the three icing algorithms for specific thresholds, and the respective scores.

Keywords: Aircraft icing, NWP based algorithm, membership functions, PIREP, contingency tables, objective verification

Contents

- Acknowledgments vii
- Resumo ix
- Abstract xi
- List of Tables xv
- List of Figures xvii
- Acronyms xix

- 1 Introduction 1**
- 1.1 Motivation 1
- 1.2 Topic Overview 2
 - 1.2.1 Ice Accretion 3
 - 1.2.2 Aerodynamic Impact 4
- 1.3 Objectives and Deliverables 4
- 1.4 Thesis Outline 5

- 2 Background 7**
- 2.1 State of the Art 7
- 2.2 IPMA Algorithm 10
- 2.3 Met Office Algorithm 11

- 3 Data and Methodology 13**
- 3.1 Data 13
 - 3.1.1 Observation 13
 - 3.1.2 The NWP model 15
- 3.2 Fuzzy Logic and Membership Functions 17
- 3.3 The icing algorithms based on NWP model 18
- 3.4 Contingency Tables and Scores 19

- 4 Results and Discussion 22**
- 4.1 Histograms 22
- 4.2 Membership functions 26
- 4.3 SFIP Algorithms 31

4.4 Contingency Tables and Scores	36
5 Conclusions	44
5.1 Future Work	46
Bibliography	47
A Supporting Figures and Tables	51

List of Tables

3.1	Characterization of the icing events.	14
3.2	Generic example of a Contingency Table.	19
4.1	Contingency Table of SFIP _{mod} algorithm forecasts for a threshold ₁ of 0.2 and a threshold ₂ of 0.3.	37
4.2	Contingency table of SFIPPT algorithm forecasts for a threshold ₁ of 0.2 and a threshold ₂ of 0.5.	39
4.3	Contingency table of SFIP algorithm forecasts for a threshold ₁ of 0.2 and a threshold ₂ of 0.35.	39
4.4	Scores attained with Tables 4.1, 4.2, and 4.3.	39
A.1	Layer forecast for each algorithm	52
A.2	Contingency Table of SFIP _{mod} algorithm forecasts for a threshold ₁ of 0.1 and a threshold ₂ of 0.1.	53
A.3	Contingency Table of SFIPPT algorithm forecasts for a threshold ₁ of 0.1 and a threshold ₂ of 0.5.	53
A.4	Contingency Table of SFIP algorithm forecasts for a threshold ₁ of 0.1 and a threshold ₂ of 0.35.	53

List of Figures

1.1	Flight Information Regions (FIR) of Lisbon and Santa Maria Oceanic.	2
3.1	Icing events' locations.	15
3.2	Monthly distribution of the icing events in terms of relative frequency.	16
3.3	Relative frequency distribution of the icing events' Average Flight Level.	16
3.4	Relative frequency distribution of the Icing Layers' Thickness.	17
4.1	Temperature (T) relative frequency distribution.	23
4.2	Cloud Liquid Water Content (CLWC) relative frequency distribution.	23
4.3	Relative Humidity (RH) relative frequency distribution.	24
4.4	Cloud Fraction (CF) relative frequency distribution.	24
4.5	Vertical Velocity relative frequency distribution.	25
4.6	Total Cloud Content (TCC) relative frequency distribution.	25
4.7	Distribution of the Thickness THICK-RH-CLWC.	26
4.8	Comparison between Temperature membership functions from SFIP _{mod} algorithm (solid blue line) and SFIPPT algorithm (dashed red line).	27
4.9	Relative Humidity membership function from SFIP _{mod} algorithm.	27
4.10	Comparison between CLWC membership functions from SFIP _{mod} algorithm (solid blue line) and SFIPPT algorithm (dashed red line).	28
4.11	TCC membership function from SFIP _{mod} algorithm.	28
4.12	Vertical Velocity membership function from SFIPPT algorithm: preliminary version (red dashed line) and updated version (blue solid line).	29
4.13	Evolution of a) Temperature and b) Relative Humidity membership functions (for SFIP _{mod}) with Flight Level (data from event no.10 of Table 3.1).	30
4.14	Evolution of a) CLWC and b) TCC membership functions (for SFIP _{mod}) with Flight Level (data from event no.10 of Table 3.1).	31
4.15	Comparison between SFIP functions for a) moderate (event no.10 of Table 3.1) and b) severe (event no.23 of Table 3.1) icing event (the black line in the figure represents the top Flight Level (FL) of the icing layer and the red line represents the bottom FL. In the case of figure b) both lines coincide).	33

4.16 Comparison between SFIP functions for a) moderate (event no.19 of Table 3.1) and b) severe (event no.24 of Table 3.1) icing event (the black line in the figure represents the top FL of the icing layer and the red line represents the bottom FL).	35
4.17 Forecast layers' thickness distribution for the SFIP, SFIP _{mod} and SFIPPT algorithms applying a 0.2 threshold to the moderate icing events.	36
4.18 Distribution of predicted layers' thickness for the SFIP, SFIP _{mod} and SFIPPT algorithms applying a 0.2 threshold to the severe icing events.	36
4.19 Probability of Detection (POD) score for the three algorithms for two different values of threshold ₁ : 0.1 and 0.2. The values displayed are based on the values of threshold ₂ that maximize True Skill Statistic (TSS) for each algorithm.	40
4.20 TSS score for the three algorithms for two different values of threshold ₁ : 0.1 and 0.2. The values displayed are based on the values of threshold ₂ that maximize TSS for each algorithm.	40
4.21 Heidke Skill Score (HSS) score for the three algorithms for two different values of threshold ₁ : 0.1 and 0.2. The values displayed are based on the values of threshold ₂ that maximize TSS for each algorithm.	41
4.22 Symmetric Extreme Dependency Score (SEDS) score for the three algorithms for two different values of threshold ₁ : 0.1 and 0.2. The values displayed are based on the values of threshold ₂ that maximize TSS for each algorithm.	41
4.23 Symmetric Extremal Dependency Index (SEDI) score for the three algorithms for two different values of threshold ₁ : 0.1 and 0.2. The values displayed are based on the values of threshold ₂ that maximize TSS for each algorithm.	42
A.1 Vertical Velocity relative frequency distribution	51

Acronyms

NWP	Numerical Weather Prediction
FAA	Federal Aviation Administration
NTSB	National Transportation Safety Board
AIRMETs	Airman's Meteorological Information
SIGMETs	Significant Meteorological Information
T	Temperature
RH	Relative Humidity
VWS	Vertical Wind Speed
POD	Probability of Detection
CLWC	Cloud Liquid Water Content
TCW	Total Cloud Water
PIREPs	Pilot Reports
AIREPs	Air-Reports
CIP	Current Icing Potential
NCAR	National Centre for Atmospheric Research
FIP	Forecast Icing Potential
IPMA	Instituto Português do Mar e da Atmosfera
SFIP	Simplified Forecast Icing Potential
WAFC	World Area Forecast Centres
MWO	Meteorological Watch Offices
FIR	Flight Information Regions
FL	Flight Level
CF	Cloud Fraction
TCC	Total Cloud Content
CIWC	Cloud Ice Water Content
TSS	True Skill Statistic

HSS	Heidke Skill Score
SEDS	Symmetric Extreme Dependency Score
SEDI	Symmetric Extremal Dependency Index
NGM	Nested-Grid Model
NAWAU	National Aviation Weather Advisory Unit
NWS	National Weather Services
SLW	Supercooled Liquid Water
SLD	Supercooled Liquid Droplets
QPF	Quantitative Precipitation Forecasts
ADWICE	Advanced Diagnosis and Warning System for Aircraft Icing Environments
DIA	Diagnostic Icing Algorithm
PIA	Prognostic Icing Algorithm
IAR	Ice Accumulation Rate
HRDPS	High Resolution Regional Deterministic Prediction System
WRF	Weather Research and Forecasting
METARs	Meteorological Aerodrome Reports
ECMWF	European Centre for Medium-Range Weather Forecasts
PNT	Previsão Numérica do Tempo

Chapter 1

Introduction

Since the first days of the civil aviation industry, one of the main concerns has been safety. In the past few decades, a lot has been done in terms of regulations, procedures, training and technology development to improve safety. Despite this, there are always factors impossible to control that affect flight safety, such as meteorological conditions. In the period from 1967 to 2010, the weather was the primary cause of the growing percentage of annual aircraft accidents. Moreover, most of the weather-related accidents occur in latitudes between 12° and 38° N/S (Mazon et al. [1]). In particular, aircraft icing is responsible for around 7, 10 and 9% of the weather-caused accidents in the climb, approach and landing phases respectively (Mazon et al. [1]) Therefore, the aviation sector has access to global gridded forecasts of major meteorological hazards to aviation, including in-flight icing (ICAO [2]), allowing aircraft to avoid hazardous environments. These forecasts are produced routinely by two World Area Forecast Centres (WAFc), known as WAFc London and WAFc Washington, operated by the Met Office and the United States National Weather Services (NWS), respectively (Bowyer and Gill [3]). These forecasts rely on the outputs of NWP models. In this thesis, the discussion revolves around NWP model outputs used to infer aircraft icing.

1.1 Motivation

Aircraft in-flight icing is defined as ice accretion on the airframe during flight. Ice accretion occurs in the presence of liquid water droplets at sub-freezing temperatures, which are most frequent in the range of -20°C to 0°C (Sand et al. [4]; Schultz and Politovich [5]), but have also been observed at temperatures down to -37.5°C in deep convective clouds (Rosenfeld and Woodley [6]). Icing conditions, and the consequent ice accretion, have a negative impact on overall aircraft performance and control, by increasing drag and weight and decreasing lift (Petty and Floyd [7]). For these reasons, aircraft in-flight icing remains to this date one of the greatest threats to aircraft operations. According to the study conducted by Green [8], in the US alone, from January 1978 to December 2002, there were 645 icing events with aerodynamic consequences for the aircraft registered in National Transportation Safety Board (NTSB) and Federal Aviation Administration (FAA) databases.

Meteorological Watch Offices (MWO) are responsible for maintaining continuous watch over meteorological conditions affecting flight operations within its area of responsibility. Moreover, MWO are responsible for preparing and disseminating Significant Meteorological Information (SIGMETs)¹ (Airman's Meteorological Information (AIRMETs)²) when severe (moderate) icing occurred, or is expected to occur (ICAO [2]). In particular, IPMA, as a MWO, is responsible to perform these tasks for two Flight Information Regions (FIR): Lisbon (EUR Region) and Santa Maria Oceanic (NAT Region), which cover an area of about 6 million km² (see Figure 1.1).

Although it is true that de-icing equipment has undergone tremendous improvements in recent years, the best way to prevent incidents and accidents related to icing events is to avoid the areas where icing is known to be occurring or may occur (Dillingham [9]). For these reasons, algorithms based on NWP models are extremely important for forecasting the areas where icing is likely to occur.

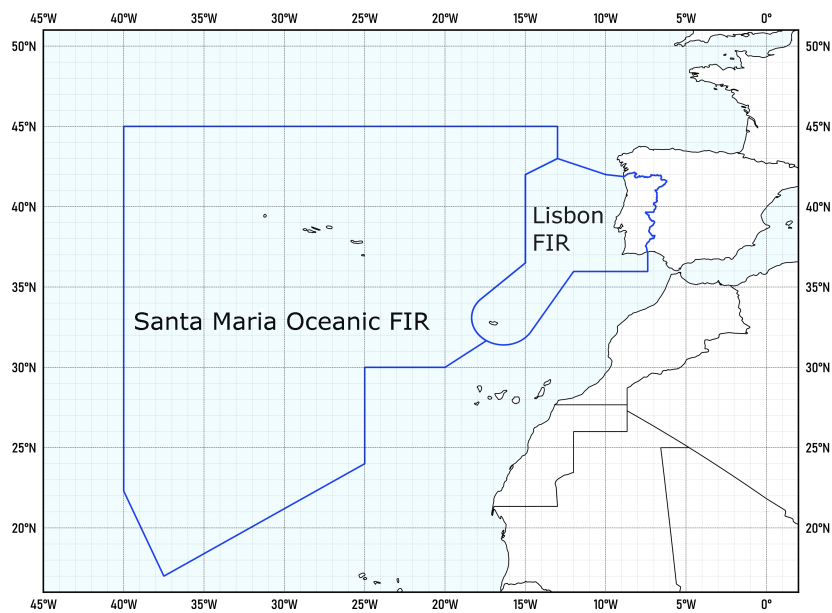


Figure 1.1: FIR of Lisbon and Santa Maria Oceanic.

1.2 Topic Overview

Algorithms used to infer aircraft icing are still to this day a work in progress. The early algorithms were based on simple atmospheric variables like Temperature (T), and Relative Humidity (RH) which, through various methods, made possible the forecasting of icing conditions (Schultz and Politovich [5], Thompson et al. [10]). However, an inter-comparison study made by Thompson et al. [10] showed that, although these algorithms have a considerably high Probability of Detection (POD), they tend to over forecast the extent of the icing areas.

¹**SIGMET information.** Information issued by a meteorological watch office concerning the occurrence or expected occurrence of specified en-route weather and other phenomena in the atmosphere that may affect the safety of aircraft operations.

²**AIRMET information.** Information issued by a meteorological watch office concerning the occurrence or expected occurrence of specified en-route weather phenomena that may affect the safety of low-level aircraft operations, and which was not already included in the forecast issued for low-level flights in the flight information region concerned or sub-area thereof.

To address this issue, icing algorithms have become more complex over the years. Recent algorithms include information from Cloud Liquid Water Content (CLWC) or Total Cloud Water (TCW), satellite and radar observations, and Pilot Reports (PIREPs). One such example is the Current Icing Potential (CIP) algorithm developed at the National Centre for Atmospheric Research (NCAR) described by Bernstein et al. [11] that applies fuzzy logic and decision tree logic to "estimate the potential for the presence of supercooled liquid water and supercooled large droplets within a given airspace", which is a necessary condition for ice accretion to take place. Later, a forecast algorithm called Forecast Icing Potential (FIP) was developed at NCAR based on the CIP approach (McDonough et al. [12]). This allowed meteorologists to forecast the icing potential in certain areas instead of diagnosing them as was done by the CIP algorithm.

More recently, Belo-Pereira [13] at IPMA, Portugal, developed a simplified version of the FIP algorithm, called SFIP, which is based on the combination of fixed membership functions for each NWP model output. Afterwards, this algorithm was adapted at the Met Office (Morcrette et al. [14]). These two versions of the Simplified Forecast Icing Potential (SFIP) will be discussed further on the next sections.

1.2.1 Ice Accretion

Ice accretion takes place in the presence of liquid water at subfreezing temperatures, as said before. Water droplets in these conditions are called supercooled droplets and have been observed in stratiform clouds (Cober et al. [15]), lenticular clouds (J. and Miloshevich [16]), cumulus clouds (Isaac and Schemenauer [17]) and deep convective clouds (Rosenfeld and Woodley [6]). Radiometer and lidar measurements showed that supercooled water clouds are mostly observed over the ocean near the storm-track regions and over land rarely occur between 40°S and 40°N (Hu et al. [18]). Supercooled droplets often appear as a thin layer at the cloud tops (Rauber and Tokay [19]). This layer was shown to be approximately 30 m deep by Cooper and Vali [20].

Rauber and Tokay [19] tried to find an explanation for the existence of water in these conditions at the upper levels of clouds. Their studies showed that "Supercooled water develops within a parcel of air containing ice crystals when the relative humidity with respect to water exceeds saturation and the condensate supply rate exceeds the bulk ice crystal mass diffusional growth rate". In other words, supercooled water develops when the air is supersaturated with water vapor and the rate at which this vapor condensates surpasses the rate at which ice crystals can grow within a certain parcel of air. Another conclusion of Rauber and Tokay [19] studies is that one important factor for the development of this liquid layer is the existence of updrafts. The required intensity of these updrafts increases as the temperature decreases.

According to Schultz and Politovich [5], upon contact of supercooled water droplets with an aircraft's aerodynamic surface, two scenarios are possible. In the first, the supercooled water droplets freeze immediately, creating a layer of rough and opaque ice, known as rime icing. Generally, this type of ice

does not pose a great threat because it has poor adhesion to the airframe and can be easily detected. The second scenario occurs when the droplets spread on impact and freeze afterward, forming glacier ice on the airframe. This type of icing is called clear icing and is associated with larger droplets in an environment with higher supercooled water content. Clear icing alters the shape of the airfoil the most, and, so, is the most dangerous form of icing (Hansman [21]). If the aircraft continues to fly in these conditions, this layer tends to grow from leading edges and over upper and lower surfaces towards the trailing edges. In certain conditions both forms of icing can develop in a process called mixed icing. In the next subsection the aerodynamic consequences of ice accretion processes are discussed.

1.2.2 Aerodynamic Impact

The accumulation of ice on the aerodynamic surfaces of an aircraft alters the shape of said surfaces, thus altering their aerodynamic performance usually by decreasing lift and increasing drag. In the case of ice accumulation on control surfaces this can mean the decrease or loss of control effectiveness (Cao et al. [22]).

The changes in the airfoil shape also tend to increase the stall speed of the aircraft which, combined with the loss of control effectiveness mentioned, can have catastrophic consequences. This is why it is important to provide airplanes with envelope protection systems in order to ensure that it is flown within its limits in icing conditions and to train pilots to deal with these situations.

To quantify the aerodynamic impact of icing, Politovich [23] at NCAR conducted a series of flights over some areas of the United States (Northeastern Colorado, Northern California and Northern Arizona) with an instrumented research King Air 200T aircraft. After analyzing the data they concluded that the maximum lift decrease was 35% and the maximum drag increase was 230% of the value in the same conditions but in the absence of ice accretion. They also detected a reduction of climb capability of 6.9 m/s. These values depict very well the dangers of aircraft icing and justify the need for continuing the development of better icing algorithms.

1.3 Objectives and Deliverables

The main objective of this thesis is to increase the knowledge about the icing environment in the Western European region. This knowledge is helpful to improve the icing algorithms based on membership functions (similar to the SFIP algorithm referred to in section 1.2) that uses NWP model outputs to predict aircraft icing. The icing environment will be characterized through histograms that depict the distribution of the most relevant atmospheric variables. This contributes to an improved setting of the thresholds used in the membership functions. Moreover, one new algorithm will be compared with other two alternatives: one that is being currently used in Portugal by IPMA (Belo-Pereira [13]) and the other implemented by the Met Office (Morcrette et al. [14]), in the UK. This comparison is performed using contingency tables for different thresholds for the value of each SFIP version.

This work also aims at giving the reader the basics of how ice accretion on aircraft aerodynamic surfaces takes place and its effects on these surfaces' aerodynamic performance, and consequently, on the aircraft operations and safety.

1.4 Thesis Outline

The remainder of this dissertation is structured in the following manner: Chapter 2 presents an overview of the state of the art regarding icing algorithms based on NWP model outputs by presenting the evolution of icing algorithms throughout the years, and analysing the current algorithm used in Portugal by IPMA and the algorithm used by the Met Office, in the UK. In Chapter 3 an explanation of the implementation put in place to solve the problem proposed is given beginning with the clarification of the data base, and then proceeding with the introduction of the fuzzy logic and membership functions concepts, and the contingency tables and scores concepts, alongside a brief explanation. The new algorithm's structure is also presented in this Chapter. Chapter 4 starts with the characterization of the icing environment with histograms showing the distribution of the atmospheric variables used in the development of the new icing algorithm. Moreover, the membership functions used in the new algorithm are explained and compared with the functions implemented in the IPMA algorithm. The results are then analyzed and discussed in depth with the help of specific examples of the application of the algorithms to events from the data base, and contingency tables derived for the three icing algorithms for specific thresholds, and the scores attained with those tables, used to assess the ability of the three icing algorithms to distinguish between moderate and severe icing. Finally, in Chapter 5 the main conclusions are drawn, and suggestions of future work are provided.

Chapter 2

Background

In this section, an overview of the evolution of icing algorithms and of the state of the art is made. Moreover, the algorithms currently operational in Portugal (IPMA - SFIPPT hereafter) and in the UK (Met Office - SFIP hereafter) are presented and explained. These algorithms will be used later to compare results with the algorithm developed in this work.

2.1 State of the Art

As already mentioned, several aircraft icing algorithms have been developed and improved over the last decades. In the early 90's, Schultz and Politovich [5] developed an automated procedure based on the outputs from a NWP model, the Nested-Grid Model (NGM), and manual techniques used by forecasters at the time at the National Aviation Weather Advisory Unit (NAWAU). This work was done with the help of a database consisting of a year's PIREPs from various types of aircraft and locations and the corresponding forecasts of temperature, relative humidity, and vertical velocity from the NWP model. The algorithm considered two levels of icing threat defined by different thresholds of temperature and relative humidity: Class 1 defined areas where icing is likely, given the cloud formation, considering $-20^{\circ}C < T < 0^{\circ}C$ and $RH > 50\%$; Class 2 was more restrictive, as an attempt to reduce forecast areas and, consequently, the number of false alarms, and indicated a greater threat of icing, considering $-15^{\circ}C < T < -2^{\circ}C$ and $RH > 65\%$. After analyzing the results, they concluded that forecasts for Class 1 criteria were of better quality than the forecasts for Class 2, regarding the miss rate, since Class 1 criteria missed about a quarter of the PIREPs, while Class 2 criteria missed approximately 50%. They also concluded that the algorithm performed best during winter and spring (seasons with greater icing threat) and that there was little degradation of quality as the lead time increased. Overall, despite having a similar miss rate as the manual procedures, the algorithm allowed for the forecasters to be liberated from the high workload task of manually analyzing the outputs from the NGM model for the risk regions, and opened doors for successive improvements in the quality of these types of algorithms (Schultz and Politovich [5]).

Bernstein et al. [11] developed the Current Icing Potential (CIP) algorithm in the late 90's, as an improvement of the previous index and others of its kind. CIP became operational in 2002 as an official product of the FAA and National Weather Services (NWS). This new algorithm took a different approach than using hard thresholds to infer icing likelihood. This new approach considers the transition from non-icing to icing environments as a gradual process and, therefore, it adopts the use of membership functions to mimic this transition. In addition, CIP combines observations from satellites, radar, surface, lightning and PIREPs with outputs from NWP models. The principal forecast variables used are temperature, relative humidity, liquid water content and vertical velocity. These predictors are combined using fuzzy logic and decision tree techniques to determine the likelihood of icing and Supercooled Liquid Droplets (SLD) at each location. As it will be discussed in Chapter 3, fuzzy logic is able to mimic the gradual transition from non-icing to icing environments through the implementation of membership functions for each relevant forecast output. After comparing the results from the algorithm against in-flight data from a research aircraft and PIREPs, they concluded that the CIP index provided users with accurate and high-resolution estimates of icing and SLD potential (Bernstein et al. [11]).

The Forecast Icing Potential (FIP) algorithm, developed at the NCAR by Mcdonough et al. [12] (2004), is independent of the use of observations. Therefore, it can provide forecasts of the icing potential several hours in advance. This allows pilots and ground staff to adapt the flight plans to the levels of icing threat further in advance, making flights safer and more efficient. The FIP algorithm uses the same structure as the CIP algorithm, but substitutes the observations of cloud and precipitation, cloud structure and precipitation type by their forecasts for the grid points of interest, which are obtained using other variables such as temperature, relative humidity, and Quantitative Precipitation Forecasts (QPF). Combining these inputs using fuzzy logic and decision trees, interest maps for the icing likelihood were built, providing a forecast of the potential for icing conditions. After analyzing the results, they concluded that the FIP algorithm provided good quality forecasts, valuable to pilots and ground staff. However, there was still margin for improvement regarding, for example, the implementation of an icing severity algorithm, given that the FIP algorithm provided icing potential forecasts without information about the severity of the icing conditions (Mcdonough et al. [12]). A similar concept was later implemented by Gencer et al. [24] in Turkey in 2010. They developed a software based on fuzzy logic and its membership functions to forecast the icing potential probability using NWP model outputs in the Turkish territory.

More recently, Belo-Pereira [13] (2015) and Morcrette et al. [14] (2019) applied a simplified version of the FIP index (named SFIP) in Portugal and in the United Kingdom, respectively. Contrary to the FIP index, this simplified version does not use forecasts relative to precipitation, cloud structure and cloud top temperature, neither applies decision trees. As it will be shown in the next two Sections, the forecasts from this index rely solely on fuzzy logic membership functions.

In Europe, other tools were developed at the same time. One such example is the Advanced Diagnosis and Warning System for Aircraft Icing Environments (ADWICE) developed in Germany. This system

identifies atmospheric regions with conditions conducive to icing, more specifically, regions where supercooled liquid water is present, using two different algorithms: the Prognostic Icing Algorithm (PIA), which allows for the forecast of areas with existing icing threat, and the Diagnostic Icing Algorithm (DIA), which combines the forecast made by the previous algorithm with observations and remote sensing data to infer the current level of icing threat (Kalinka et al. [25]). Both algorithms rely on NWP model outputs. ADWICE forecasts cover Europe and the Mediterranean coast of North Africa with 30 vertical hybrid levels and a horizontal grid spacing of 7km. The combination of a prognostic part (PIA) and a diagnostic part (DIA), and the recent addition of satellite data to the latter, improved the short-term forecast quality by reducing the over-forecasting of icing conditions and, consequently, the false alarm rate (Kalinka et al. [25]).

Recently, Boudala et al. [26] (2019) performed a study in Canada to gain a better understanding of the conditions associated with aircraft icing. This study was motivated by the fact that icing was reported frequently in the region of Cold Lake, Alberta, but forecasting these events proved to be a challenge. Thus, several ground-based instruments were deployed in that area, including the weather sensors already present at the Cold Lake airport, during the 2016/2017 winter season. PIREPs of that area during said period and the respective observations data were also analyzed. To forecast these conditions, two aircraft icing intensity algorithms based on an Ice Accumulation Rate (IAR) for a cylindrical shape moving at a given airspeed were tested. This cylindrical shape was used as an approximation of an airfoil (Boudala et al. [26]). The algorithms were named IAR_1 and IAR_2 , and the difference between them is that IAR_1 takes into consideration the density of ice, whereas the IAR_2 algorithm does not. The input forecasts were obtained from the Canadian High Resolution Regional Deterministic Prediction System (HRDPS), which produces forecasts for the Canadian territory with a 2.5 km horizontal resolution and a vertical resolution that varies between 110 m near the surface to 4 km at a 40 km altitude (Boudala et al. [26]). Both algorithms were tested for two different values of airspeed: 89 ms^{-1} and 60 ms^{-1} . After comparing the predictions against the PIREPs, they concluded that the IAR_1 was not able to correctly forecast icing conditions for that region using the inputs from the HRDPS model, probably because the model showed an overestimation of liquid water content. On the other hand, the IAR_2 algorithm with the lower airspeed showed some skill in forecasting light icing, which represented 76% of the reported icing events, with a tendency to underestimate the moderate icing events (Boudala et al. [26]).

Also in 2019, Thompson [27] conducted a study in the United States to assess the skill of an NWP model, called Weather Research and Forecasting (WRF) (Skamarock and Klemp [28]), in forecasting icing conditions on the ground and in the air by comparing the model results against PIREPs, data from research aircraft and surface observations reported in Meteorological Aerodrome Reports (METARs). To conduct this study, a database of about 9000 observations of icing conditions from research aircraft flights was made available by the FAA. Moreover, 280.000 icing PIREPs reported for a 6 month period (from October to April) from 2001 to 2011 were compiled, including PIREPs reporting the lack of icing conditions, as well as 3.4 million METARs for the same 10-year period. Instead of running simulations

for each date and location of all the reports collected, a simulation covering the entire US territory for a 13-year period starting on October 1st 2000 was run (Thompson [27]). Comparing the model simulations with all the data available, the WRF model proved to be highly skilful in predicting icing conditions on the ground and in the air. In particular, this study indicated that the more severe the reported event was, the higher the likelihood of the model forecasting the presence of Supercooled Liquid Water (SLW). Concerning surface precipitation (rain and snow), ground icing events (freezing drizzle and freezing rain) and the occurrence of ice pellets, the model showed promising skill with approximately 60% of these events being correctly forecast. However, the model skill decreases in the spring and fall seasons. This is probably due to the fact that weather conditions have a higher variability during this time of year, which makes correct forecasts harder to achieve (Thompson [27]).

One thing that these algorithms have in common is the comparison of the forecasts against PIREPs. However, PIREPs have some shortcomings worth mentioning such as the fact that the content of the PIREPs is left at the pilot's discretion, the reported severity of the event is subjective because it is determined by the pilot, and the reported location of the event is often inaccurate (Schwartz [29]). Moreover, the transmission is not obligatory, which means that not all events are reported, and there is a distribution bias, since pilots try to avoid areas with icing conditions and reports are naturally more frequent in areas with higher air traffic density, and a category bias towards positive events, since the non-occurrence of icing is rarely reported (Kalinka et al. [25]). That said, PIREPs are still the only widely and readily available independent source of information regarding the presence (or absence) of icing conditions (Kalinka et al. [25]).

2.2 IPMA Algorithm

The algorithm developed at IPMA, described by Equation 2.1, consists of a simplified version of the FIP algorithm (McDonough et al. [12]). It is based on fuzzy logic and membership functions. This algorithm results from the combination of membership functions applied to the NWP model outputs considered relevant (Belo-Pereira [13]). The weighing factors used in Equation 2.1 are $a = 0.35$, $b = 0.2$ and $c = 0.45$.

$$SFIPPT = M_T(a \times M_{RH} + b \times M_w + c \times M_{LWC}) \quad (2.1)$$

Equation 2.2 represents the membership function of temperature

$$M_T = \begin{cases} 0, & \text{if } T \leq T_1 \\ \frac{T-T_1}{T_2-T_1}, & \text{if } T_1 < T \leq T_2 \\ 1, & \text{if } T_2 < T \leq T_3 \\ 1 - \left(\frac{T-T_3}{T_4-T_3} \right), & \text{if } T_3 < T \leq T_4 \\ 0, & \text{if } T > T_4 \end{cases} \quad (2.2)$$

with $T_1 = -28^\circ C$, $T_2 = -12^\circ C$, $T_3 = -1^\circ C$ and $T_4 = 1^\circ C$. Equation 2.3 represents the membership function of Relative Humidity

$$M_{RH} = \begin{cases} 0, & \text{if } RH \leq RH_1 \\ \left(\frac{RH - RH_1}{RH_2 - RH_1} \right)^2, & \text{if } RH_1 < RH \leq RH_2 \\ 1, & \text{if } RH > RH_2 \end{cases} \quad (2.3)$$

with $RH_1 = 0.6$ and $RH_2 = 0.95$.

The shape of the functions 2.2 and 2.3 will be discussed in Section 4.2. Note that previously for flight levels below FL050 a slightly different function was used in Belo-Pereira [13] (her Figure 4). Presently, the same functions are used for all levels.

The membership function for cloud liquid water is defined as follows:

$$M_{CLW} = \begin{cases} \frac{CLW}{0.4}, & \text{if } CLW \leq 0.4gkg^{-1} \\ 1.0, & \text{if } CLW > 0.4gkg^{-1} \end{cases} \quad (2.4)$$

Presently, the vertical velocity membership function is defined by Equation 2.5. This is different from the version described in Belo-Pereira [13] (her Figure 4). The differences will be discussed in Section 4.2.

$$M_w = \begin{cases} 1, & \text{if } w < -0.5 \text{ } Pas^{-1} \\ -2w, & \text{if } -0.5 \leq w < -0.0001 \text{ } Pas^{-1} \\ 0, & \text{if } w \geq -0.0001 \text{ } Pas^{-1} \end{cases} \quad (2.5)$$

2.3 Met Office Algorithm

The algorithm implemented at Met Office (SFIP) was adapted from Belo-Pereira [13]. The differences between the two algorithms concern the membership function for vertical velocity (Morcrette et al. [14], Figure 2) and the fact that in Morcrette et al. [14] all membership functions are independent of the flight level, in contrast to those implemented by Belo-Pereira [13].

Morcrette et al. [14] evaluated the new index against satellite data and ground based remote sensing observations. This study showed that the new index outperforms the icing index previously used operationally by the London WAFC.

Chapter 3

Data and Methodology

In this chapter, an overview of the data used is presented, distinguishing between the observed data and the data obtained from an NWP model, which is briefly explained. The association of both enables a complete description of the icing events considered in the database. The fuzzy logic and membership functions concepts, and the contingency tables and scores concepts are introduced and explained. Furthermore, the new algorithm built to infer aircraft icing is presented and explained, establishing the link between the database and each membership function used in the algorithm.

3.1 Data

As mentioned before, this study uses observation and model data. The observation consists of special Air-Reports (AIREPs) of icing. It is important to note that, in this text, the terms AIREPs and PIREPs are used synonymously despite their minor differences. The model data is from the European Centre for Medium-Range Weather Forecasts (ECMWF) deterministic model. This model is explained in greater detail in Subsection 3.1.2.

3.1.1 Observation

The observations used in this study include 27 icing events reported over the Iberian Peninsula, the Balearic Sea, the United Kingdom, Ireland, and the Azores (see Figure 3.1(a)). Since there is a high density of events over the south-east of the Iberian Peninsula and the Balearic Sea, a detailed view of this region is given in Figure 3.1(b). The AIREPs include the information about the severity of icing, the flight level of the base and the top of the icing layer. They also include information of location, time, and dates.

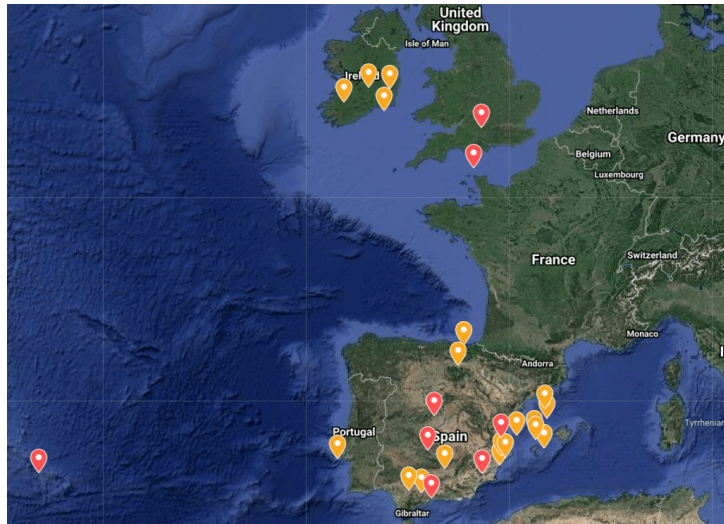
Concerning the monthly distribution of the events, Figure 3.2 shows that most of the icing events took place during wintertime. This is more notorious for severe icing events, which is expected since the atmospheric conditions conducive to icing events are more common during winter months.

Table 3.1: Characterization of the icing events.

Event No.	Severity	Date (dd/mm/aa)	Time (hh:mm)	Latitude (°)	Longitude (°)
1	moderate	20/11/2020	08:05	52.75	-6.68
2	moderate	04/12/2020	13:10	37.05	-4.93
3	moderate	10/12/2020	06:35	38.27	-0.57
4	moderate	15/12/2020	18:55	52.00	-7.00
5	moderate	18/12/2020	07:51	52.30	-9.18
6	moderate	28/12/2020	10:08	39.53	0.37
7	moderate	24/04/2021	14:50	38.15	-3.62
8	moderate	21/05/2021	06:52	52.80	-7.83
9	moderate	28/05/2021	08:00	39.60	1.37
10	moderate	03/12/2020	21:12	43.30	-2.55
11	moderate	04/12/2020	13:05	38.70	-0.47
12	moderate	04/12/2020	16:10	37.17	-5.62
13	moderate	28/12/2020	10:20	40.27	2.08
14	moderate	28/12/2020	10:32	38.63	-0.25
15	moderate	08/03/2021	15:35	42.45	-2.87
16	moderate	18/03/2021	16:32	38.98	1.87
17	moderate	17/04/2021	10:19	39.37	1.40
18	moderate	22/04/2021	11:11	40.68	1.92
19	moderate	25/11/2020	09:16	38.55	-9.52
20	severe	30/11/2020	14:15	51.42	-1.58
21	severe	09/12/2020	10:45	50.00	-2.00
22	severe	10/12/2020	07:00	39.48	-0.47
23	severe	10/12/2020	11:30	36.80	-4.37
24	severe	20/01/2021	10:43	38.93	-4.55
25	severe	09/02/2021	13:20	37.90	-1.55
26	severe	19/02/2021	18:08	37.92	-26.10
27	severe	13/05/2021	08:35	40.37	-4.23

Figure 3.3 shows the relative frequency of the average flight level of the icing events. According to this Figure, almost 90% of the moderate events and 63% of the severe events occurred between FL 050 and FL 200. Nearly 37% of the severe icing events occurred above FL200. It is interesting to note that the lapse rate is commonly 6°C/km and, for instance, in the Lisbon area, the average temperature at 2m is 10.5°C in January (Portal do Clima [30]). This indicates that the layer in the range 0°C to -20°C, favourable to the presence of supercooled water droplets, lies between FL055 and FL165. Moreover, also in Lisbon area, in May, the average temperature at 2m is 15.3°C. So, in this case, the layer favourable to the formation of supercooled water lies between FL085 and FL200. Thus, it is understandable that the majority of the icing events occurred between FL050 and FL200.

Figure 3.4 depicts the distribution of the icing layers' thickness. The histogram shows that around 88% of the severe icing reports had a thickness inferior to 1000 ft. This suggests severe icing events tend to occur in a thinner layer rather than throughout a broad icing layer. Moreover, the velocity at which the aircraft goes through the flight levels with conditions conducive to icing can be of such magnitude that the observed icing layers appear to be smaller than the actual layers where these conditions are,



(a) Pan view of the icing events.



(b) Detailed view of the icing events over the Iberian Peninsula.

Figure 3.1: Icing events' locations.

in fact, present. In contrast, most of the moderate events (approximately 74%) occurred for a thickness varying between 1000 ft and 10000 ft, with a more expressive percentage between 1000 and 2000 ft.

3.1.2 The NWP model

As said previously, the forecast data is provided by the ECMWF deterministic model. This model is based on a cubic-octahedral spectral transform discretization, which corresponds to a grid spacing of approximately 9 km. The model consists on a transformation, based on Fourier and Legendre transforms, from the grid-point space to a 'spectral' space where each variable (field) is discretized and represented by the sum of analytical functions, the spherical harmonics. Finally, each field is transformed back to the grid-point space and its real value is computed (Malardel et al. [31]). This model has 137 vertical levels, with the height of the lowest level around 10 m above ground. In the troposphere,

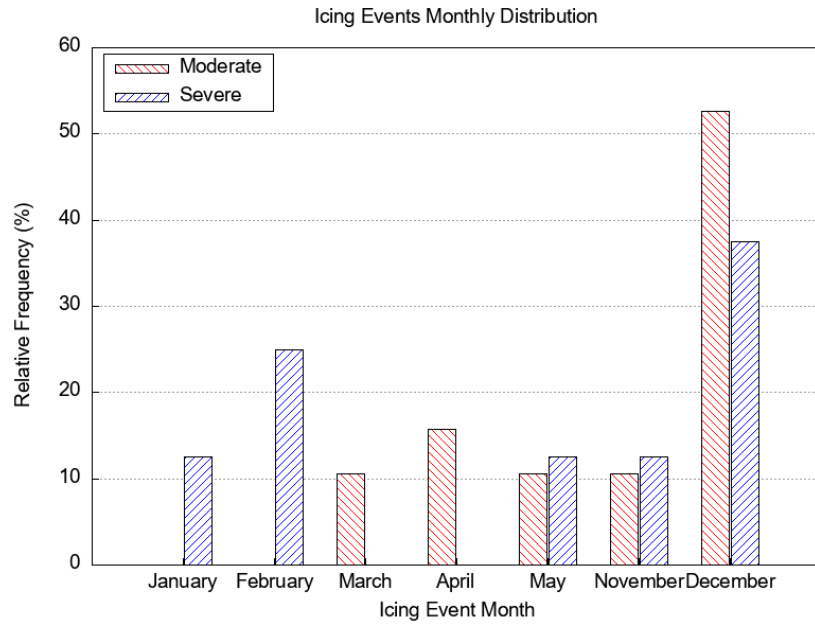


Figure 3.2: Monthly distribution of the icing events in terms of relative frequency.

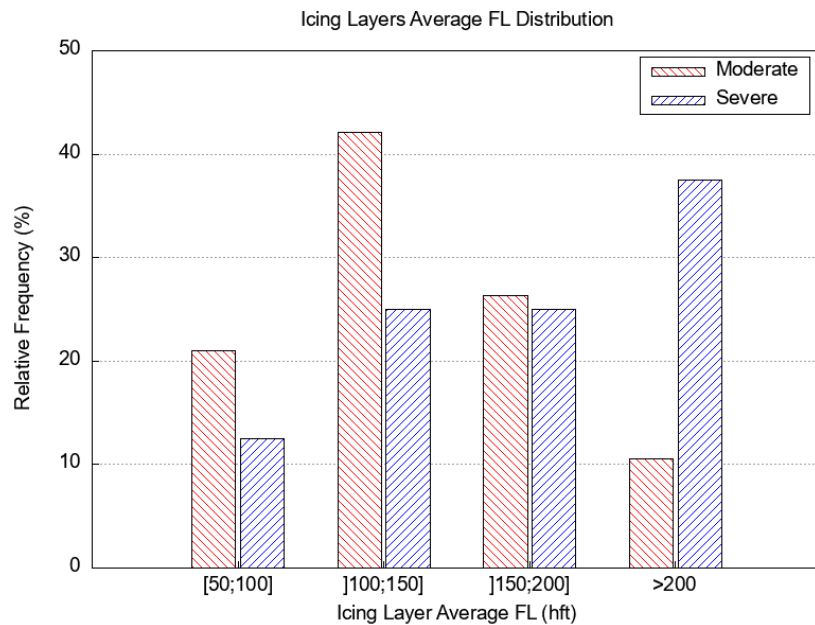


Figure 3.3: Relative frequency distribution of the icing events' Average Flight Level.

the vertical grid-spacing increases from 20 m near the surface to 290 m above 6 km. In this study, the analyzed variables are Temperature (T), Cloud Liquid Water Content (CLWC), Relative Humidity (RH), Cloud Fraction (CF), Vertical Velocity and Total Cloud Content (TCC). Each model variable was extracted for the closest grid point of the model near the location of the icing reports, using the forecasts with a lead-time of 12 hours.

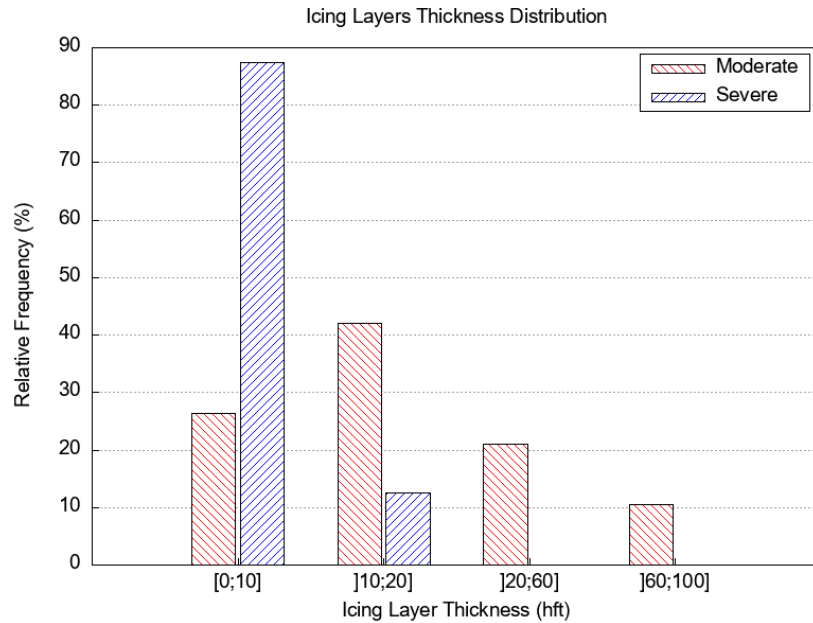


Figure 3.4: Relative frequency distribution of the Icing Layers' Thickness.

3.2 Fuzzy Logic and Membership Functions

The concept of Fuzzy Logic was first introduced by Lotfi Zadeh in 1965, but its application in environmental sciences only gained visibility in the early 1990s following the work done by MIT Lincoln Laboratory in 1993 and the NCAR in 1994, where fuzzy logic algorithms were developed for detecting gust fronts and microbursts, from Doppler radar data (Williams [32]).

Fuzzy logic tries to mimic the human approach to solving a certain problem, specially those where the decisions do not follow a sequence of well-defined logical statements, which represent most of the problems posed to human experts, by accommodating and even taking advantage of the ambiguity of human language, since several concepts used in everyday language do not have clear definitions and/or boundaries (Williams [32]).

While in classical logic a given concept is either in a set or outside the set, fuzzy logic allows for this membership to be partial. Thus, fuzzy Logic can also be interpreted as an extension of classical logic, where boundaries are well defined, to fuzzy sets and their manipulation (Williams [32]). The degree to which a particular concept belongs to a fuzzy set is given by its respective Membership Function. These functions range from 0 to 1 and are often defined by experience and knowledge. In the case of the icing algorithms they rely on the comparison between NWP models' outputs, and the icing PIREPs and on the forecasters' experience. For this reason it makes sense to use this kind of functions in icing forecast algorithms (as presented in the following section).

In the context of icing forecasts, membership functions depict the gradual transition from icing to non-icing environments by determining the icing likelihood depending on a certain forecast variable (Bernstein et al. [11]). As previously explained, the variables of interest for the new algorithm developed are Temperature (T), Cloud Liquid Water Content (CLWC), Relative Humidity (RH), Cloud Fraction (CF)

and Total Cloud Content (TCC).

3.3 The icing algorithms based on NWP model

The analysis of the predictors' distribution, that will be presented Section 4.1, represents the first step necessary to improve the icing algorithms. In the present section, a new algorithm (hereby called SFIP_{mod} - Modified SFIP) is explained.

This new algorithm, described by Equation (3.1), follows the same line of thought as the algorithms from IPMA and the Met Office presented in Chapter 2. It uses membership functions to combine the information of the relevant variables, each weighted by the respective coefficients, except for the membership function of Temperature. Explaining in more detail, $f_m(T)$ represents the membership function of the Temperature, $f(RH)$ the membership function of Relative Humidity, $f(tcc)$ the membership function of the Total Water Content, and $f_m(CLWC)$ the membership function of Cloud Liquid Water Content. In terms of coefficients, cr , ctc and cc are the coefficients of RH, TCC and CLWC (respectively), and assume the values of 0.35, 0.2 and 0.45 in the same order, as in Belo-Pereira [13]. Other values were tested but it was decided to use these ones because they attained the best results.

$$SFIP_{mod} = f_m(T)(cr \times f(RH) + ctc \times f(tcc) + cc \times f_m(CLWC)) \quad (3.1)$$

$$f_m(T) = \begin{cases} 0, & \text{if } T \leq -28^\circ C \\ \frac{T - (-28)}{-16 - (-28)}, & \text{if } -28^\circ C < T \leq -16^\circ C \\ 1, & \text{if } -16^\circ C < T \leq -2^\circ C \\ 1 - \left(\frac{T - (-2)}{1 - (-2)} \right), & \text{if } -2^\circ C < T \leq 1^\circ C \\ 0, & \text{if } T > 1^\circ C \end{cases} \quad (3.2)$$

$$f(RH) = \begin{cases} 0, & \text{if } RH \leq 0.6 \\ \left(\frac{RH - 0.6}{0.95 - 0.6} \right)^2, & \text{if } 0.6 < RH \leq 0.95 \\ 1, & \text{if } RH > 0.95 \end{cases} \quad (3.3)$$

Considering the work done by Belo-Pereira [13] and Morcrette et al. [14], understanding the membership functions of Temperature (3.2) and Relative Humidity (3.3) is straight forward. The major difference lies in the TCC (3.4) and CLWC (3.5) membership functions. For the latter, an exponential evolution was adopted instead of the linear evolution used by the mentioned authors. In the case of the TCC membership function, it was introduced as a substitute for the Vertical Velocity membership functions implemented by Belo-Pereira [13] and Morcrette et al. [14].

$$f(tcc) = \begin{cases} 1.475 \times tcc^{0.3065}, & \text{if } tcc < 0.2813g/kg \\ 1, & \text{if } tcc \geq 0.2813g/kg \end{cases} \quad (3.4)$$

$$f_m(CLWC) = \begin{cases} 1.475 \times CLWC^{0.3065}, & \text{if } CLWC < 0.2813g/kg \\ 1, & \text{if } CLWC \geq 0.2813g/kg \end{cases} \quad (3.5)$$

The thresholds of each function will be explained in the next Chapter (Section 4.2) where the analysis of the functions is made in more detail using the plots of the functions for sets of theoretical values.

3.4 Contingency Tables and Scores

There are several methods available to evaluate the performance of forecast models. However, contingency tables and the scores associated to them are the most frequent tools used to assess the quality of a forecast model or algorithm (Thornes and Stephenson [33]; Gold et al. [34]). Hence, these tables and scores are used in this work to evaluate the forecasting skill of the algorithm built.

A contingency table is a two by two table that shows the relation between the forecast of any given event by a forecast model (or algorithm) and the observation of said event (icing events in the specific case of this dissertation). Table 3.2 shows a generic example of a contingency table. In this table, entry "A" is the number of events that were forecast and observed. In other words, it represents the number of correct forecasts (hits). Entry "B" represents the number of events that were forecast but were not observed (false alarms), and constitutes a Type 2 error (Thornes and Stephenson [33]). Entry "C" represents the number of events that were not forecast but were observed (misses), and constitutes a Type 1 error ([33]). Finally, entry "D" is the number of events that were neither forecast nor observed, which are also considered correct forecasts (correct negative forecasts).

Table 3.2: Generic example of a Contingency Table.

Forecast	Observation	
	Yes	No
Yes	A	B
No	C	D

In terms of the scores, from the several scores that can be determined from a contingency table (Doswell et al. [35]), five different scores are used to assess the performance of the SFIP_{mod} algorithm. These are: Probability of Detection (POD), True Skill Statistic (TSS), Heidke Skill Score (HSS), Symmetric Extreme Dependency Score (SEDS), and Symmetric Extremal Dependency Index (SEDI).

The fraction of correctly forecast events given by equation 3.6 is defined as Probability of Detection (POD) (Doswell et al. [35]) or as hit rate (Ferro and Stephenson [36]).

$$POD = \frac{A}{A + C} \quad (3.6)$$

The True Skill Statistic (TSS), also known as Hanssen-Kuipers (H-K) Discriminant (Belo-Pereira [37]), is defined by equation 3.7. This score "compares the number of correct forecasts, minus those attributable to random guessing, to that of a hypothetical set of perfect forecasts" (Doswell et al. [35]).

$$TSS = POD - POFD \quad (3.7)$$

where $POFD = B/(B + D)$ corresponds to the probability of false detection, which is defined as the ratio of false alarms to the total number of nonevents.

The Heidke Skill Score (HSS) is given by equation 3.8

$$HSS = \frac{C - E}{N - E} \quad (3.8)$$

where $C = A + D$ is the number of correct forecasts, N is the sample size and $E = [(A + B)(A + C) + (B + D)(C + D)]/N$ is the expected number of correct forecasts due solely to chance (Doswell et al. [35]).

Some previous studies (Doswell et al. [35], Hogan et al. [38], Stephenson et al. [39]) have shown that many scores based on 2x2 contingency tables, including the ones mentioned above, converge to trivial values (0 or 1) as the rarity of the events increases, i.e., when the observations of non-events dominate the contingency table. To overcome some of the drawbacks of these scores, other verification measures have been derived, namely the Symmetric Extreme Dependency Score (SEDS) suggested by Hogan et al. [38], defined as:

$$SEDS = \frac{\log(q) - \log(POD)}{\log(BR) + \log(POD)} \quad (3.9)$$

where $q = (A + B)/N$ is the relative frequency with which the event was forecast, N is the sample size, and $BR = (A + C)/N$ is known as the base rate and corresponds to the relative frequency of occurrence of the event.

More recently, Ferro and Stephenson [36] proposed the Symmetric Extremal Dependency Index (SEDI) given by equation 3.10.

$$SEDI = \frac{\log(POFD) - \log(POD) + \log(1 - POD) - \log(1 - POFD)}{\log(POD) + \log(POFD) + \log(1 - POD) + \log(1 - POFD)} \quad (3.10)$$

It is important to note that, to evaluate a certain forecast algorithm, one should use a set of different scores rather than a single score because, as it will be discussed in Section 4.4, the scores are sensible to different factors.

Chapter 4

Results and Discussion

This Chapter starts with the presentation and discussion of the distribution of the relevant atmospheric variables based on the forecasts from the ECMWF model relative to the icing events from the database. Moreover, the results are discussed in detail, namely the membership functions, the comparison between the three SFIP algorithms addressed in this thesis, the contingency tables derived for these algorithms and the scores obtained. These scores will allow to draw conclusions about the performance of each algorithm concerning the ability to discriminate between moderate and severe icing events.

4.1 Histograms

In this section the distribution of Temperature, Cloud Liquid Water Content (CLWC), Relative Humidity (RH), Cloud Fraction (CF), Vertical Velocity and Total Cloud Content (TCC) based on forecasts of the ECMWF model outputs are presented and discussed. Figure 4.1 depicts the distribution of the predicted temperature for the icing events. As expected, the majority of the moderate events happened at temperatures between -20°C and 0°C . Moreover, nearly 70% of the severe events took place at temperatures between -24°C and -8°C . The histogram also shows that a considerable percentage (approximately 44%) of the severe events occurred for temperatures lower than -20°C . This is possible because, in the absence of sufficient ice nuclei, liquid cloud droplets can still exist at temperatures between -20°C and around -40°C (Korolev et al. [40]). This result is also in agreement with other studies (Sand et al. [4]; Schultz and Politovich [5]; Rosenfeld and Woodley [6]; Marwitz et al. [41]).

Most of both moderate and severe icing events occurred for CLWC values higher than 0.0005 g/kg (Figure 4.2). Only roughly 36% of the moderate events and 23% of the severe events occurred for lower values. Moreover, nearly 60% of the severe events occurred for CLWC in the range of 0.0005 to 0.05g/kg and no severe event has values greater than 0.2g/kg .

Figure 4.3 shows that the vast majority of both moderate and severe icing events occurred for Relative Humidity values higher than 80%. For lower values the events are more or less evenly spread, until the range of values lower than 30%, where no severe events were registered and only a small percentage

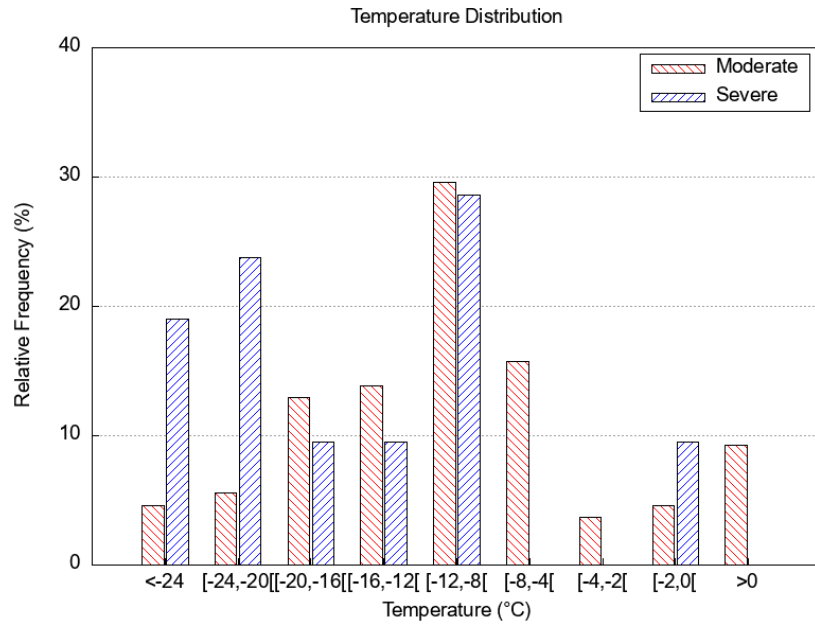


Figure 4.1: Temperature (T) relative frequency distribution.

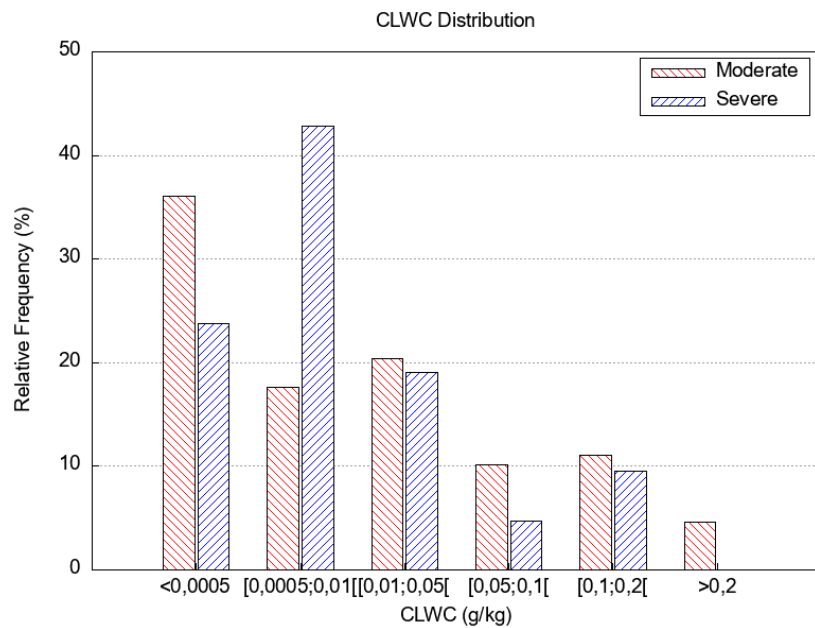


Figure 4.2: Cloud Liquid Water Content (CLWC) relative frequency distribution.

(about 13%) of moderate events took place.

The histogram of Cloud Fraction (CF) illustrated in Figure 4.4 indicates that around 74% of the moderate events and 53% of the severe events took place for CF values higher than 0.1. However, the distribution of CF is widespread, revealing a low predictive skill of this variable.

Figure 4.5 shows the distribution of the maximum Vertical Velocity (in m/s) in the troposphere, where positive values represent upward motion and negative values represent downward motion. This histogram shows that more than 50% of the severe events occurred in the presence of upward motion, favouring the cloud formation. In contrast, the majority (around 56%) of the moderate events occurred in

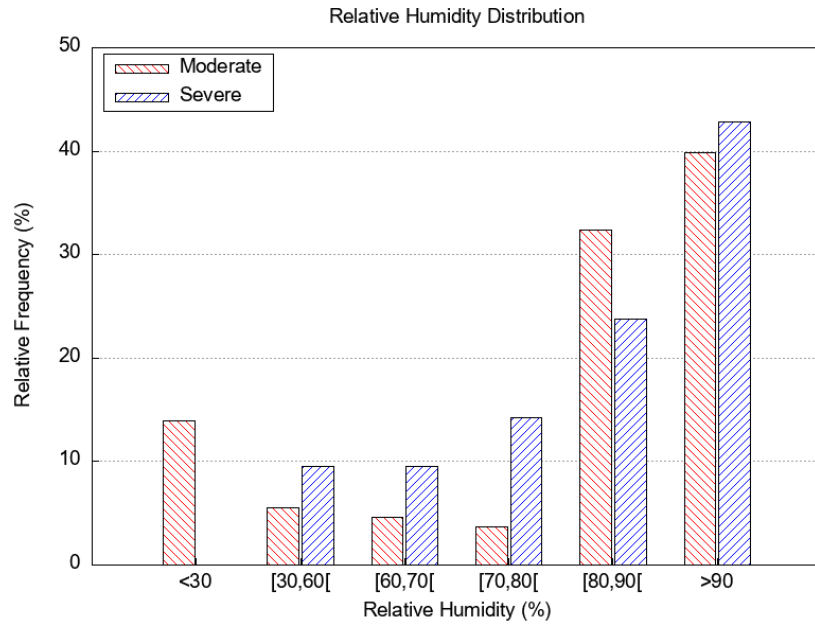


Figure 4.3: Relative Humidity (RH) relative frequency distribution.

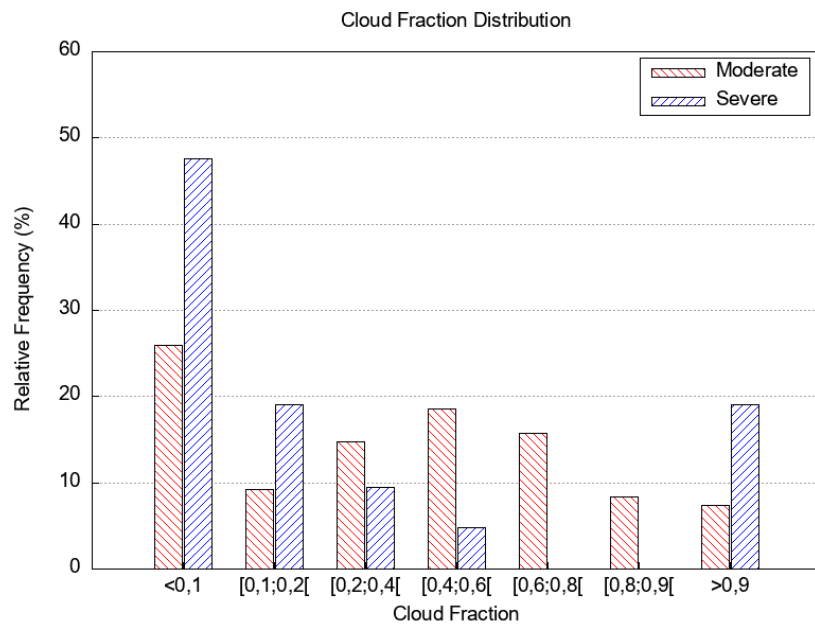


Figure 4.4: Cloud Fraction (CF) relative frequency distribution.

the presence of downward motion. This suggest that the use of the vertical velocity in the prediction of icing conditions has some limitations. A similar histogram for the Vertical Velocity but with units of Pa/s is presented in Appendix A (Figure A.1).

Figure 4.6 depicts the distribution of Total Cloud Content (TCC), which is the sum of CLWC and Cloud Ice Water Content (CIWC). From this figure, it is visible that more than half (about 58%) of the moderate events happened for TCC higher than 0.01 g/kg. Regarding severe events, around 81% of the events occurred beyond the 0.0005 g/kg threshold.

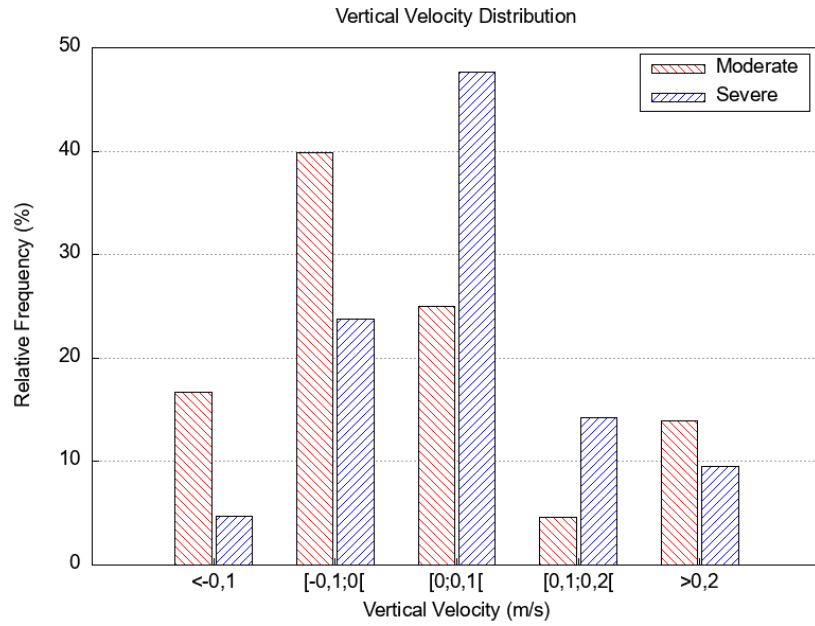


Figure 4.5: Vertical Velocity relative frequency distribution.

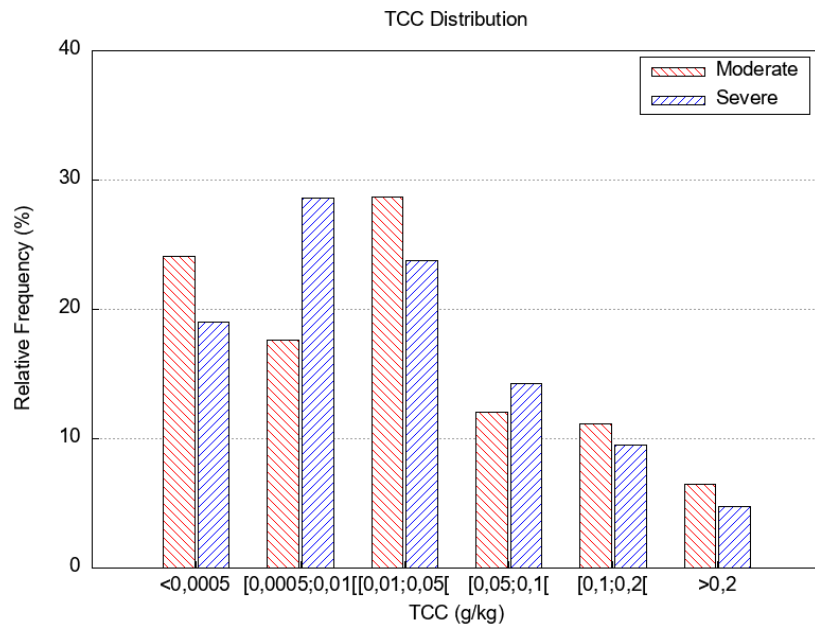


Figure 4.6: Total Cloud Content (TCC) relative frequency distribution.

Figure 4.7 shows the distribution of the thickness of the icing layer satisfying certain conditions in terms of RH and CLWC. This thickness is referred to as the THICK-RH-CLWC and is determined in three steps. The first step determines the layer (IC-RH) that satisfies this condition:

$$\cap \begin{cases} RH \geq 80\% \\ -20^{\circ}C < T \leq 0^{\circ}C \end{cases}$$

The second step determines the layer (IC-CLWC) that satisfies this condition:

$$\cap \begin{cases} CLWC \geq 0.0005g/kg \\ -20^{\circ}C < T \leq 0^{\circ}C \end{cases}$$

The final step determines the maximum layer thickness of the layers IC-CLWC and IC-RH. Figure 4.7 shows the histogram of the thickness THICK-RH-CLWC, revealing that, the majority (over 60%) of both severe and moderate icing events occurred for thicknesses between 50 hft and 100 hft. The remainder of the severe icing events happened for thicknesses lower than 50 hft. Nearly 15% of the moderate icing events took place for thicknesses higher than 100 hft. This information indicates that the thickness THICK-RH-CLWC could be a useful predictor of the conditions conducive to icing events.

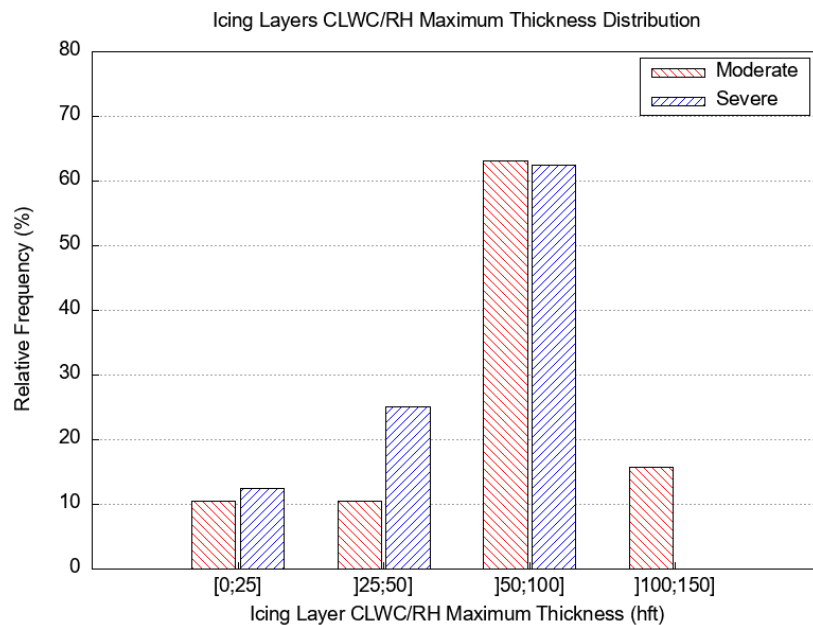


Figure 4.7: Distribution of the Thickness THICK-RH-CLWC.

4.2 Membership functions

Figure 4.8 compares the membership functions of Temperature used in SFIPPT algorithm (currently operational at IPMA) and a new function, used in the new SFIP_{mod} algorithm (see Section 3.3). According to Figure 4.1, more than 60% of the moderate icing events took place at temperatures between -16°C and -2°C. Moreover, icing events are more frequent at temperatures below -16°C than at temperatures above -2°C. The new membership function (SFIP_{mod}), shown in Figure 4.8, tries to mimic these features. Therefore, while the old function (SFIPPT) has the maximum value at temperatures between -14°C and -1°C, the new membership function reaches its maximum value at temperatures between -16°C and -2°C. Moreover, the slope for temperatures below -16°C is lower than the slope for temperatures above -2°C.

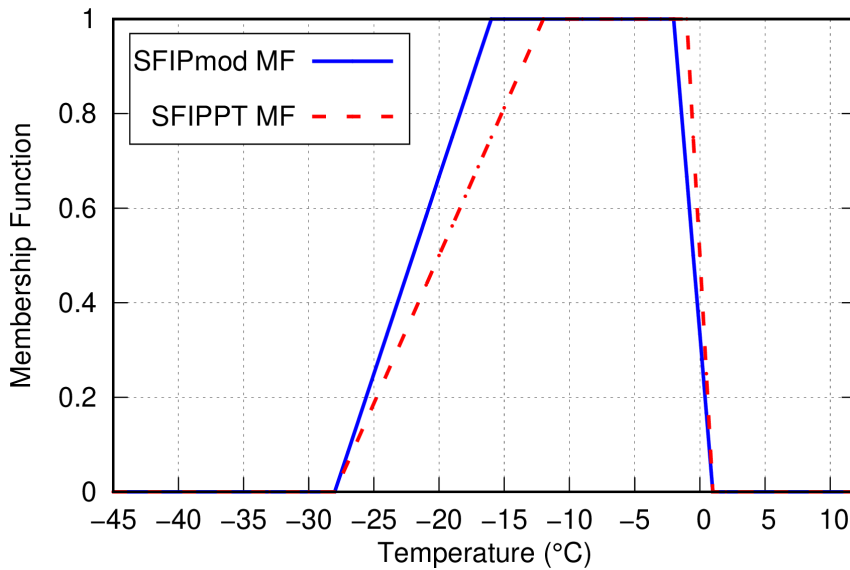


Figure 4.8: Comparison between Temperature membership functions from SFIP_{mod} algorithm (solid blue line) and SFIPPT algorithm (dashed red line).

Figure 4.9 shows the membership function of Relative Humidity from the SFIP_{mod} algorithm. The membership function implemented in the SFIPPT algorithm has the same shape, therefore is not represented in the figure. Taking into consideration the histogram of Figure 4.3, from a 60% RH value on, there is a rapid increase in the number of icing events, both moderate and severe, until the peak value is reached above the 90% threshold. The membership function depicts this feature. A rapid increase from a RH of 60% to a 95%, where the function reaches its highest value of 1.

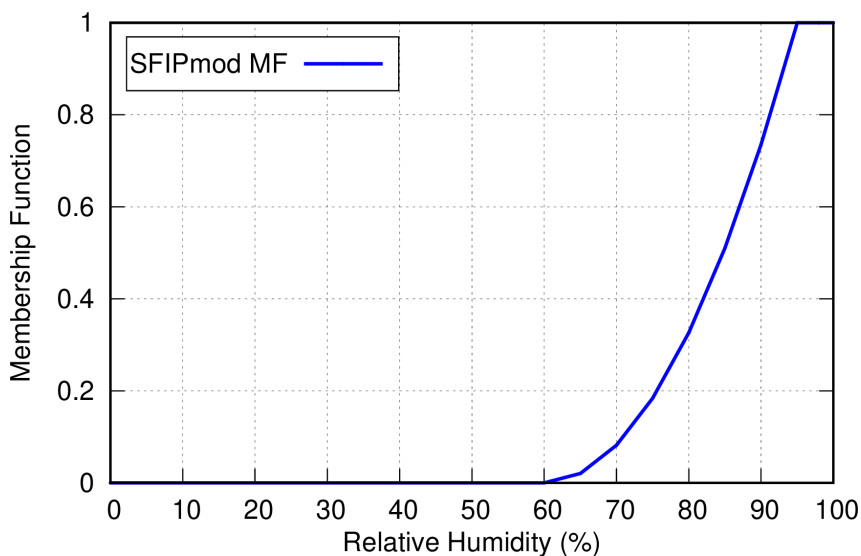


Figure 4.9: Relative Humidity membership function from SFIP_{mod} algorithm.

In subfreezing conditions, the greater the Cloud Liquid Water Content (CLWC), the higher is the quantity of supercooled water available to accrete to the aircraft's surfaces. Thus, higher values of CLWC are conducive to more severe icing conditions. The membership functions shown in Figure 4.10 mimic this feature. However, the two functions have a different growth rate with CLWC. The membership function used in the SFIPPT algorithm increases linearly, reaching the maximum value for a CLWC of

0.4 g/kg. On the other hand, the new membership function (SFIP_{mod}) increases exponentially from 0, for a CLWC of 0 g/kg, to 1, for a CLWC of 0.2813 g/kg. It is relevant to remember that over 50% of the severe and moderate icing events occur for CLWC values lower than 0.01 g/kg. For values higher than 0.01 g/kg, the number of icing events gradually decreases (Figure 4.2). The new membership function tries to reflect this feature by attributing higher membership values to lower values of CLWC, so that the new function gives more importance to lower values of CLWC when compared to the SFIPPT algorithm function.

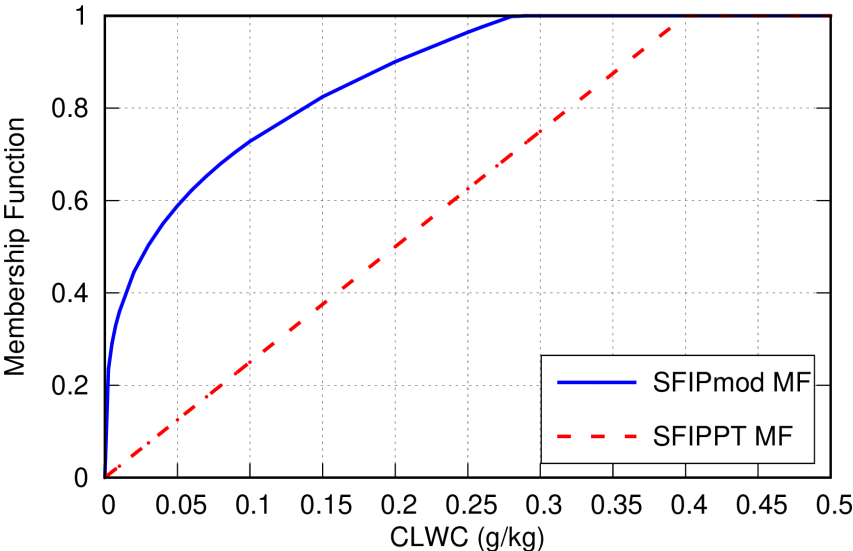


Figure 4.10: Comparison between CLWC membership functions from SFIP_{mod} algorithm (solid blue line) and SFIPPT algorithm (dashed red line).

The membership function of TCC in Figure 4.11 follows the same line of thought as the previous function. The histogram of Figure 4.6 indicates that this variable has similar features to those of CLWC. Thus, it was decided to use the same membership function.

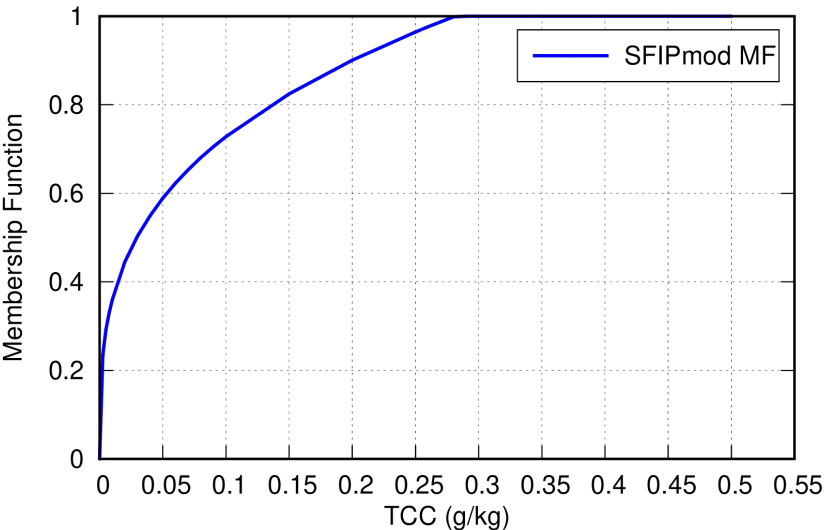


Figure 4.11: TCC membership function from SFIP_{mod} algorithm.

Figure 4.12 shows two versions of the membership function of the Vertical Velocity from the SFIPPT algorithm. It is known that the upward vertical motion favours the cloud formation, whereas the downward vertical motion favours cloud dissipation. The membership function tries to mimic these features. In its preliminary version (dashed red line), the function attributed positive values for upward motion (negative vertical velocity) and negative values for downward motion (positive vertical velocity). However, the presence of downward vertical motion does not necessarily exclude the possibility of an icing event taking place, as could be suggested by the negative membership value (see Figure 4.5). Thus, in the updated version (solid blue line) of this function it was decided to assume a membership value of 0 for downward motion.

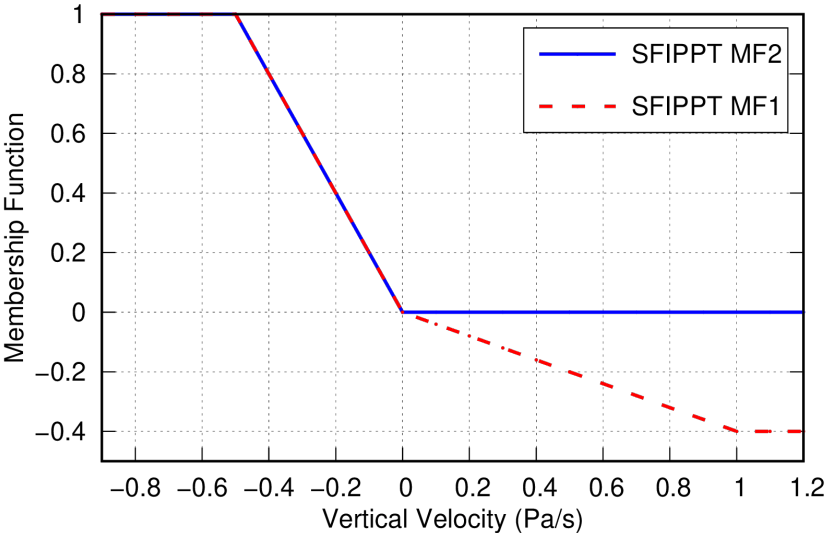


Figure 4.12: Vertical Velocity membership function from SFIPPT algorithm: preliminary version (red dashed line) and updated version (blue solid line).

Figure 4.13 shows the vertical distribution of the Temperature (Figure 4.13 a) and Relative Humidity (Figure 4.13 b) membership functions for the event no.10 (see Table 3.1). This moderate icing event was reported between Flight Levels 120 and 140. As mentioned in Section 3.2, the membership functions mimic the gradual transition from non-icing to icing environments. Thus, the function should reach its maximum value inside the icing environment which, in this case, is between FL120 and FL140. Both functions from Figure 4.13 reach their peak values within these Flight Levels.

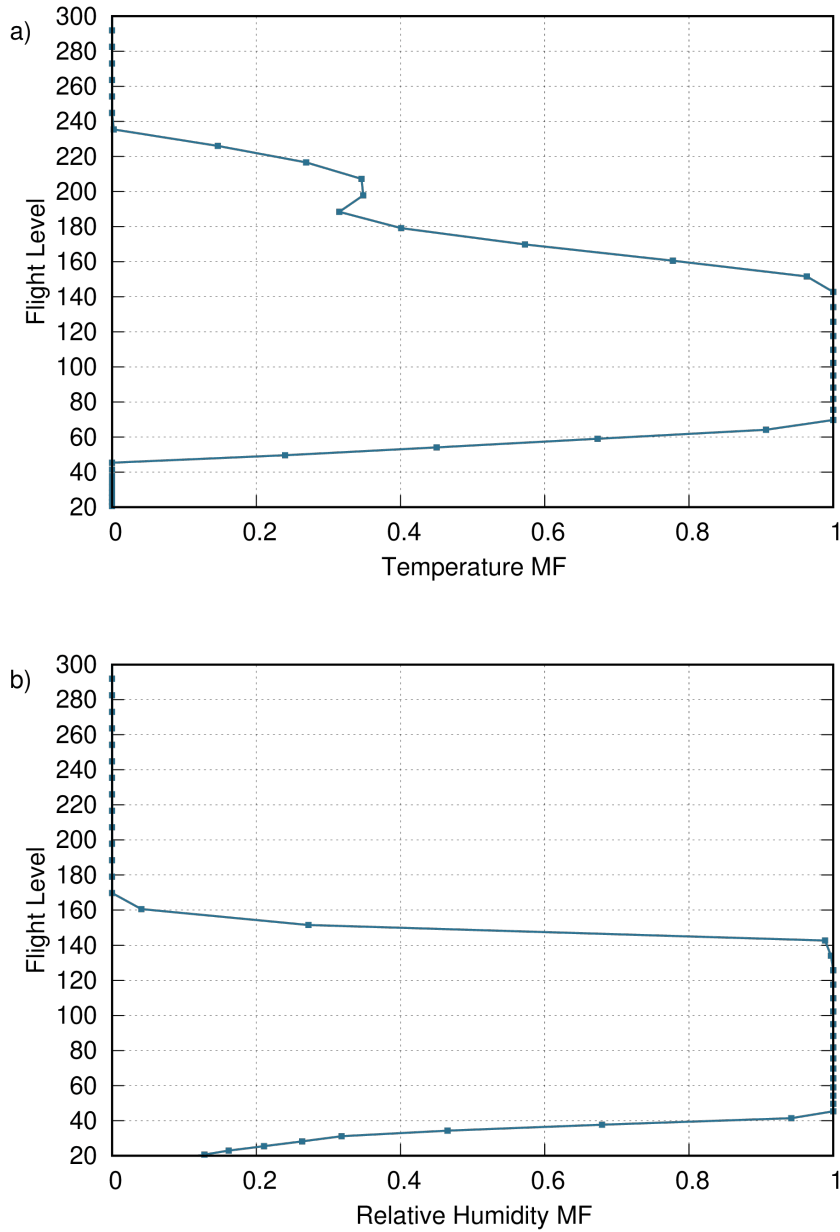


Figure 4.13: Evolution of a) Temperature and b) Relative Humidity membership functions (for SFIP_{mod}) with Flight Level (data from event no.10 of Table 3.1).

Figure 4.14 shows the vertical distribution of CLWC (Figure 4.14 a) and TCC (Figure 4.14 b) membership functions for the same event (no.10). In this case, the functions do not attain their peak value within the Flight Levels where icing was reported. Nevertheless, the functions still reach a relatively high membership value for each variable, which is considered a good result given the fact that this event was reported as a moderate icing event.

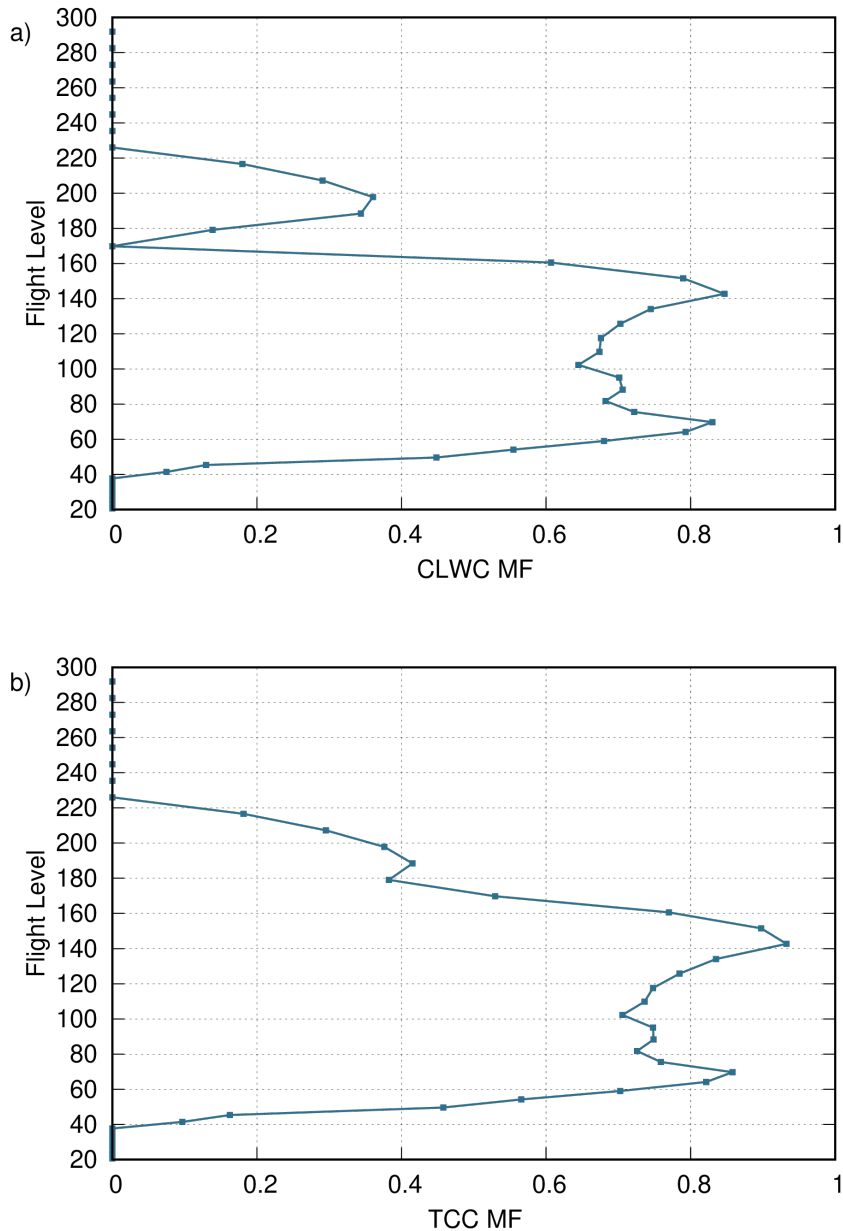


Figure 4.14: Evolution of a) CLWC and b) TCC membership functions (for $SFIP_{mod}$) with Flight Level (data from event no.10 of Table 3.1).

These results for all four membership functions suggest that these four variables are good predictors of the icing occurrence.

4.3 SFIP Algorithms

Figure 4.15 shows a comparison between the three icing forecast algorithms presented in this dissertation. In Figure 4.15 a) this comparison is made for a moderate icing event, namely, the event number 10 (see Table 3.1), which took place over the north of the Iberian Peninsula. Figure 4.15 b) presents this comparison for a severe icing event, namely, the event number 23 (Table 3.1), which occurred over the south region of the Iberian Peninsula.

Focusing on Figure 4.15 a), the three algorithms show a similar behaviour despite having different magnitudes. This influences greatly the algorithms' forecasting skill. For example, considering a threshold of 0.8, only the SFIP_{mod} algorithm is able to forecast icing. In this case, the algorithm forecasts two icing layers: one between FL070 and FL095, and the other between FL110 and FL140 (approximate Flight Levels). Although the algorithm forecasts two icing layers when only one was observed (between FL120 and FL140), it still performs well in forecasting icing conditions for the layer where it was observed. It is important to note that the fact that no icing has been reported on the bottom layer does not imply that no icing has occurred on that layer. Moreover, icing is only reported when observed by visual inspection or when detected by any of the flight systems installed for this purpose.

This analysis can be made for other thresholds. For example, using a threshold of 0.68 only the SFIP_{mod} and the SFIPPT algorithms forecast icing conditions. The first algorithm forecasts icing between FL065 and FL140 and the second between FL065 and FL070 (approximately). In this case, the SFIP_{mod} algorithm forecasts only one icing layer that includes the layer where icing was, in fact, observed but with a higher thickness than using the 0.8 threshold. The SFIPPT algorithm, in turn, forecasts icing conditions within two flight levels that are much lower than the flight levels where the icing event actually took place. So, in this particular case, the SFIPPT algorithm fails to forecast this icing event.

Finally, using a threshold of 0.2 all three algorithms are able to forecast icing conditions. The SFIP algorithm forecasts one icing layer between FL060 and FL150, the SFIP_{mod} algorithm forecasts one icing layer between FL055 and FL160 and the SFIPPT algorithm forecasts one icing layer between FL050 and FL150. All predicted layers include the layer of the event and, in all cases, the observation is located in the upper half of the predicted layers. This information is also available in Table A.1, where the analysis for the 0.2 threshold value is presented for all icing events. This discussion illustrates the importance of the choice of the thresholds.

Concerning Figure 4.15 b), the three algorithms once again show a similar behaviour with different peak values. However, this event is slightly different from the previous one because the icing event was reported for a single flight level (FL160). Starting again with a 0.8 threshold, the only algorithm capable of forecasting icing conditions is the SFIP_{mod}, and it forecasts these conditions between FL130 and FL150 (approximately). Although the predicted icing layer does not include the reported flight level, this can be considered a reasonable result due to the proximity between the predicted layer and the reported flight level (FL160). Besides, the icing conditions may have started at lower levels.

Changing to a threshold of 0.52, both the SFIP_{mod} and the SFIPPT algorithms forecast icing conditions. The first algorithm forecasts icing between FL110 and FL155 and the second between FL150 and FL155 (approximately). In this case, the SFIP_{mod} forecasts icing conditions within a larger layer than the previous example, and the forecast gets closer to the reported FL. The SFIPPT algorithm also forecasts icing within a single layer that is close to the reported FL, but the predicted layer is much thinner than the one forecast by the SFIP_{mod} algorithm.

Finally, once again, with a 0.2 threshold, all three algorithms forecast icing conditions. The SFIP algorithm forecasts one icing layer between FL140 and FL150, the SFIP_{mod} forecasts one icing layer between FL100 and FL165 and the SFIPPT forecasts one icing layer between FL100 and FL185. In this situation, the layer predicted by the SFIP algorithm does not include the reported FL, but the top FL of the forecast layer is close to the observed, which is still a reasonable result. The SFIP_{mod} algorithm forecasts icing conditions within a larger layer than for the previous threshold value. This layer includes the reported flight level. The SFIPPT algorithm also forecasts a single icing layer that is much larger than the previous example. This time, the forecast layer is thicker than the one predicted by the SFIP_{mod} algorithm.

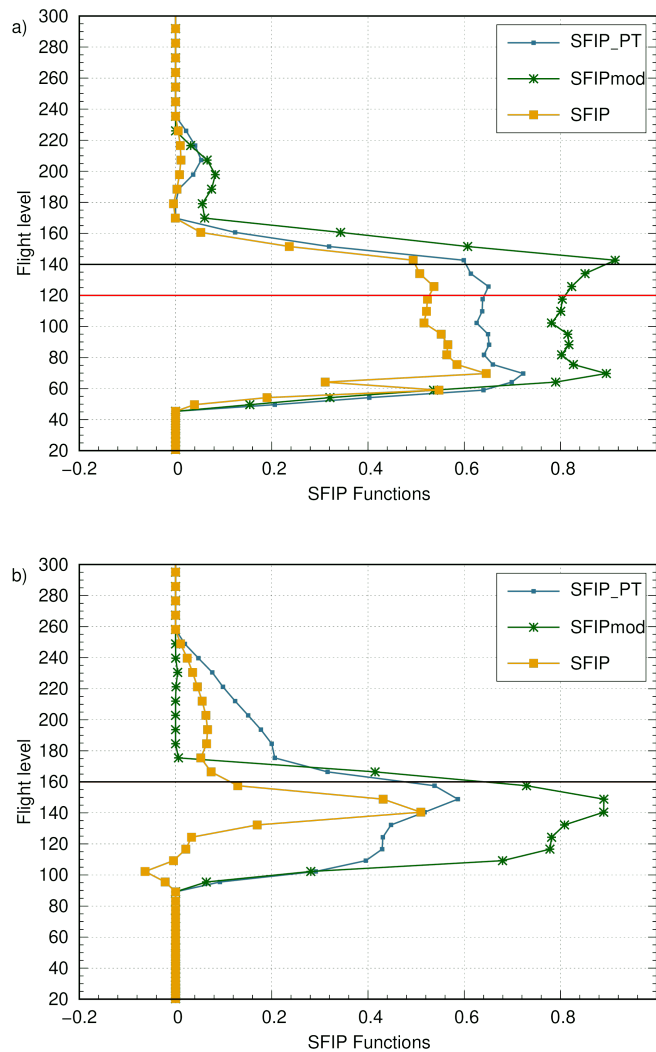


Figure 4.15: Comparison between SFIP functions for a) moderate (event no.10 of Table 3.1) and b) severe (event no.23 of Table 3.1) icing event (the black line in the figure represents the top FL of the icing layer and the red line represents the bottom FL. In the case of figure b) both lines coincide).

Figure 4.16 shows a comparison between the three icing forecast algorithms, for two other events. The first event, a moderate icing event (panel a) took place in the Lisbon FIR near Cascais and was reported between FL060 and FL080 (event 19, Table 3.1). Figure 4.16 b) illustrates the comparison for a severe icing event, more specifically, the event number 24 from Table 3.1, which occurred over Spain

near Ciudad Real and was reported between FL170 and FL190.

As in the previous examples, the three functions have a similar shape but with different maximum values (Figure 4.16 a). For a threshold of 0.8, the SFIP_{mod} is the only algorithm that forecasts icing conditions, in particular, for the layer from FL130 to FL150 (approximately), which is considerably above the icing layer reported. So, for this threshold, this algorithm performs poorly.

For a threshold of 0.68, the SFIP_{mod} forecasts icing conditions between FL130 and FL150 and the SFIP algorithm forecasts icing between FL150 and FL160, clearly above the level where icing was observed. The SFIPPT algorithm does not forecast icing conditions for this threshold. Thus, all algorithms perform poorly.

For a threshold of 0.2 all three algorithms are able to forecast icing conditions. The SFIP_{mod} algorithm indicates the existence of icing conditions between FL070 and FL100 and between FL115 and FL170. The SFIPPT algorithm forecasts icing between FL070 and FL095 and between FL125 and FL160. These two algorithms forecast two icing layers that include about half of the reported layer in the lower layers. Despite this, the percentage of intersection between the predicted and the observed layers is considerably small, so both algorithms perform poorly. The SFIP algorithm, on the other hand, forecasts one icing layer between FL125 and FL180, that is much higher than the observed layer. Thus, this algorithm also shows a poor performance for this threshold. Overall, all the algorithms perform poorly for this specific icing event.

Figure 4.16 b) shows that the three algorithms are incapable of predicting icing conditions in the layer where severe icing was reported. Moreover, all predicted icing for threshold higher than 0.2 is on a layer below the reported one. As in the previous examples, the thickness of this layer is larger for the SFIP_{mod} algorithm than for the other algorithms. The disparity between the reported and the predicted levels is of nearly 8000 ft. There are several factors that can explain this result. For instance, the climb rate of the aircraft could be of such magnitude that the ice accretion was reported passed the region with icing conditions. It is also possible that the NWP model used could be over forecasting the presence of CLWC at the region where icing was forecast, since the accuracy of the predictions of quantities like CLWC from these models still poses a challenge (Boudala et al. [26]).

Figure 4.17 shows the distribution of the icing layers' thickness predicted by the three algorithms, for the moderate icing events. A threshold of 0.2 was applied for these forecasts. This figure indicates that almost 70% of the predicted layers by the SFIP algorithm have a thickness inferior to 10 hft. Concerning the SFIP_{mod} algorithm, nearly 70% of the predicted icing layers have a thickness greater than 60 hft and about 5% have a thickness smaller than 10 hft. Concerning the SFIPPT algorithm, approximately 42% of the forecast icing layers have a thickness greater than 60 hft. Another 42% of these forecasts indicate an icing layer's thickness between 20 hft (excluding) and 60 hft (including). Thus, it is clear that, the SFIP algorithm tends to forecast layers with a relatively smaller thickness than the other algorithms. On the other hand, the SFIP_{mod} tends to forecast icing layers with higher thicknesses.

Figure 4.18 shows the same distributions as the previous figure but for the severe icing events. This

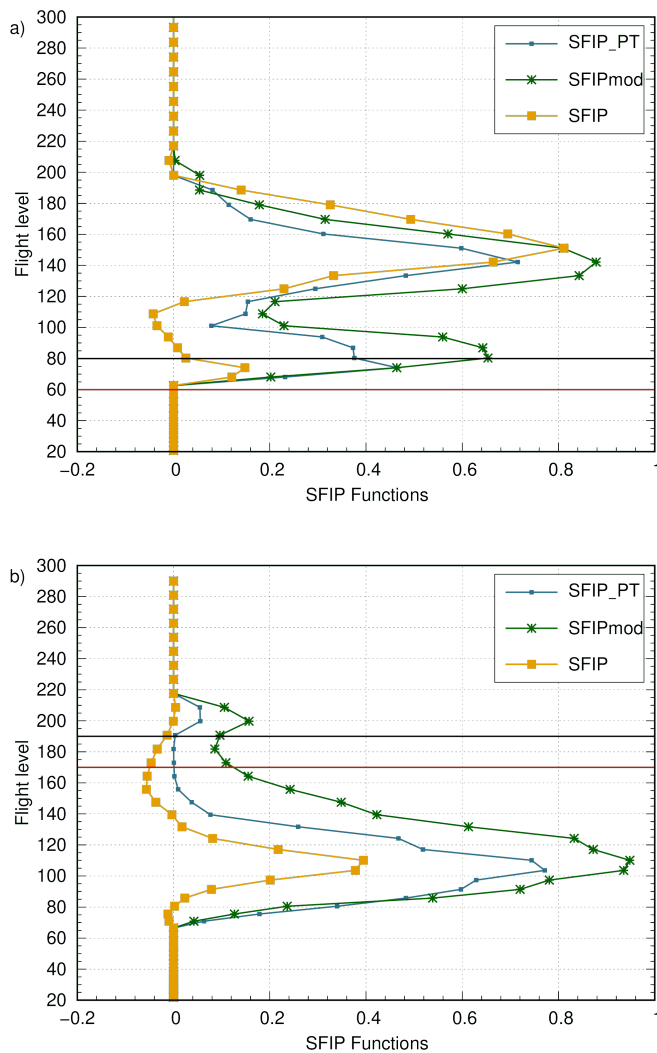


Figure 4.16: Comparison between SFIP functions for a) moderate (event no.19 of Table 3.1) and b) severe (event no.24 of Table 3.1) icing event (the black line in the figure represents the top FL of the icing layer and the red line represents the bottom FL).

figure illustrates similarities with the previous figure. Namely, for the SFIP above 60% of the forecasts have a layer's thickness inferior to 10 hft, while the other algorithms forecast small thicknesses only in less that 15% of the severe icing events. The SFIPPT algorithm forecasts thicknesses greater than 60 hft for almost 40% of the severe icing events, and the SFIP_{mod} predicts thicknesses greater than 60 hft for more than 60% of the severe icing events.

It is relevant to note some differences between the figures 4.17 and 4.18. For the severe icing events, only one algorithm predicts thicknesses larger than 100 hft, namely, the SFIP_{mod} algorithm. Furthermore, for the severe icing, the percentage of cases with a thickness inferior to 10 hft is higher than when considering the moderate icing events.

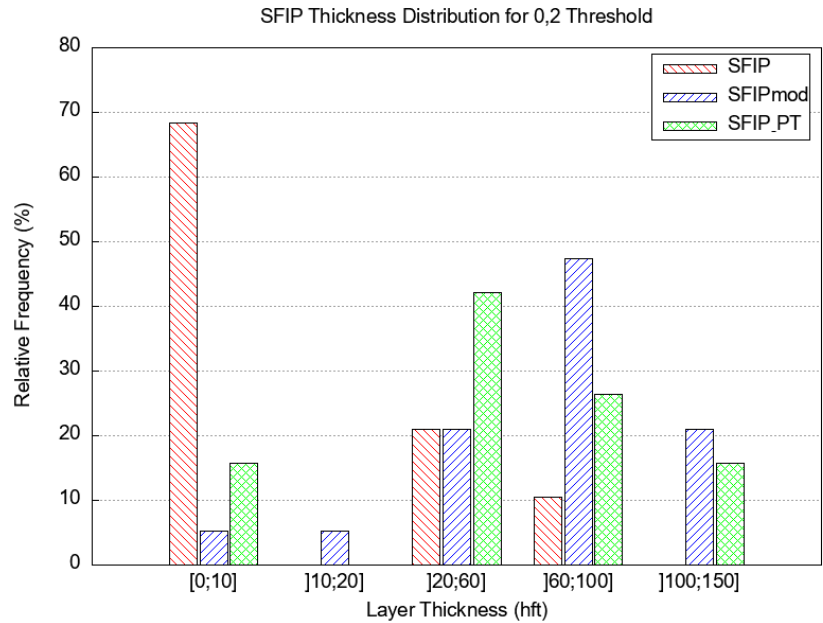


Figure 4.17: Forecast layers' thickness distribution for the SFIP, SFIP_{mod} and SFIPPT algorithms applying a 0.2 threshold to the moderate icing events.

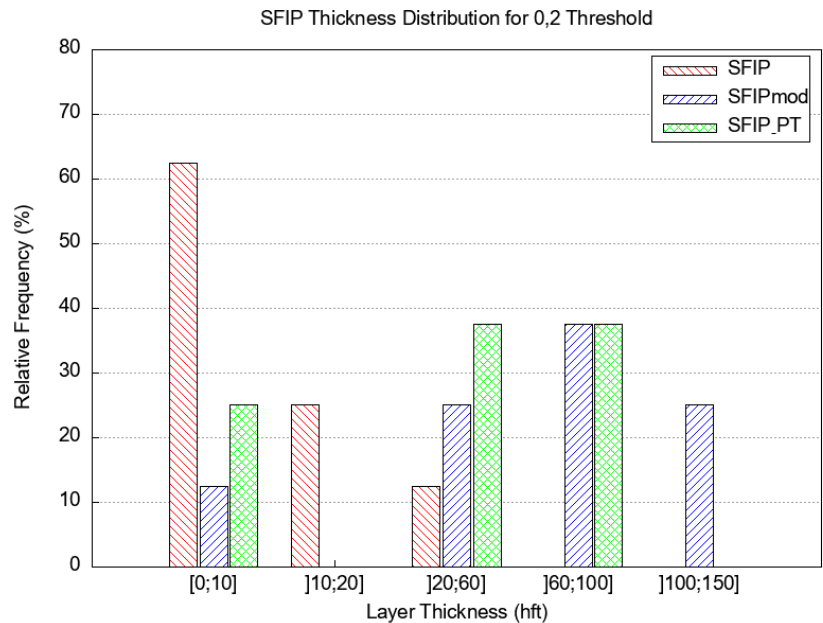


Figure 4.18: Distribution of predicted layers' thickness for the SFIP, SFIP_{mod} and SFIPPT algorithms applying a 0.2 threshold to the severe icing events.

4.4 Contingency Tables and Scores

In this section, it is presented the analysis of the contingency tables derived for the three icing algorithms for specific thresholds, and the scores attained with those tables, to assess the ability of the three icing algorithms to distinguish between moderate and severe icing. Moreover, an explanation is given concerning how these tables were built and the meaning of the scores associated with them in the context of the problem at hand.

Table 4.1 shows a contingency table built using the forecasts applying the SFIP_{mod} algorithm. For this specific case, a "yes" forecast or observation corresponds to a severe icing event, and a "no" forecast or observation corresponds to a moderate icing event or absence of icing. This table indicates that this algorithm has 6 hits or correct forecasts, 13 false alarms (also referred to as a Type 2 error in Section 3.4), 2 misses (also referred to as a Type 1 error in Section 3.4) and 6 correct negative forecasts. In other words, the table indicates 6 instances where a severe icing event was forecast and reported (hit), 13 instances where a severe icing event was forecast but not observed (false alarm), 2 occurrences where a severe icing event was not forecast but was reported (miss) and 6 occurrences where a severe icing event was neither forecast nor reported (correct negative). Thus, the number of false alarms dominates this table.

Table 4.1: Contingency Table of SFIP_{mod} algorithm forecasts for a threshold₁ of 0.2 and a threshold₂ of 0.3.

Forecast	Observation	
	Yes	No
Yes	6	13
No	2	6

The construction of the contingency tables depends on a series of criteria, which are listed and explained below. Moreover, to demonstrate the application of these criteria, examples from Figures 4.15 and 4.16 as well as Table 4.1 (and its thresholds) will be used.

The criteria applied to define a hit are:

- The percentage of intersection between the forecast layer and the reported layer should be higher than 40%, or the distance between the predicted layer and the single-level report should be inferior to 1000 ft;
- The maximum value of the algorithm should be greater than threshold₂;
- The severity of the observed event should be severe.

Figure 4.15 b) serves as an example to illustrate a hit. According to the figure, for a threshold₁ (threshold of the first criterion) of 0.2, the predicted layer includes the reported flight level. In addition, the maximum value of the SFIP_{mod} algorithm is higher than the threshold₂ (threshold of the second criterion) of 0.3. Finally, the event was reported as severe. Thus, all criteria defining a hit are fulfilled.

False alarms are the defined by the following set of criteria:

- The percentage of intersection between the forecast layer and the reported layer should be higher than 40%, or the distance between the predicted layer and the single-level report should be inferior to 1000 ft.

- The maximum value of the algorithm should be greater than threshold_2 .
- The severity of the observed event has to be reported as moderate.

An example of a false alarm is given by Figure 4.15 a). The figure shows that for a threshold_1 of 0.2, the forecast layer includes the reported layer in its entirety. Moreover, the maximum value of the SFIP_{mod} algorithm is higher than 0.3 (threshold_2). Lastly, the severity of the event was reported as moderate. Therefore, the criteria for a false alarm are met.

The criteria to define a miss are:

- The percentage of intersection between the forecast layer and the reported layer should be smaller than 40%, or the distance between the predicted layer and the single-level report should be greater than 1000 ft.
- The maximum value of the algorithm lower than threshold_2 .
- The severity of the observed event has to be reported as severe.

In the case of a miss, only one of the first two criteria and the third criterion must be met. For example, if the first and third criteria are met, the forecast is considered a miss regardless of the maximum value of the algorithm. This is exemplified in Figure 4.16 b). For a threshold_1 of 0.2, the forecast layer does not intercept the reported layer and the event was reported as severe. This is considered a miss, despite the fact that the maximum value of the SFIP_{mod} algorithm is higher than the threshold_2 (0.3).

Correct negative forecasts are defined by the following set of criteria:

- The percentage of intersection between the forecast layer and the reported layer should be smaller than 40%, or the distance between the predicted layer and the single-level report should be greater than 1000 ft.
- The maximum value of the algorithm lower than threshold_2 .
- The severity of the observed event has to be reported as moderate.

Correct negatives, similarly to the misses, only have to meet one of the first two criteria and the third criterion. Figure 4.16 a) serves as an example of a correct negative forecast. The figure shows that, although the forecast layer intersects the observed layer, the percentage of intersection is considerably small (nearly 11%). Thus, the first criterion is met. Furthermore, the event was reported as moderate. So, this example is a correct negative forecast.

The contingency tables were computed for the three algorithms and for four different values (0.05, 0.1, 0.15, 0.2) of the threshold_1 . Several values of the threshold_2 were also tested. Tables 4.2 and 4.3 are the contingency tables derived from the forecasts of the SFIPPT and SFIP algorithms, respectively,

for a threshold₁ of 0.2 and a threshold₂ of 0.5 and 0.35, respectively. Unlike the previous table, these tables are dominated by the correct negative forecasts.

Table 4.2: Contingency table of SFIPPT algorithm forecasts for a threshold₁ of 0.2 and a threshold₂ of 0.5.

Forecast	Observation	
	Yes	No
Yes	4	6
No	4	13

Table 4.3: Contingency table of SFIP algorithm forecasts for a threshold₁ of 0.2 and a threshold₂ of 0.35.

Forecast	Observation	
	Yes	No
Yes	2	3
No	6	16

Table 4.4 presents the scores attained with the previous contingency tables (Table 4.1, Table 4.2, and Table 4.3). The scores shown correspond to different values of threshold₂ for the different algorithms. These values of threshold₂ are those that maximize the TSS score for each case. This table shows that SFIP_{mod} algorithm has the highest probability of detection. Namely, this algorithm forecasts 75% of all the severe icing events. The other algorithms have lower probability of detection, 50% and 25%, respectively for SFIPPT and SFIP algorithms. However, the other scores reveal that SFIPPT outperforms the other algorithms and that SFIP_{mod} has the poorest skill. This is due to fact that SFIP_{mod} has the highest number of false alarms. Comparing SEDS and SEDI scores, it is noticeable that the SEDS has lower values than SEDI for all algorithms. This reflects the fact that SEDS penalizes more the over-forecasting than SEDI (Ferro and Stephenson [36]).

Table 4.4: Scores attained with Tables 4.1, 4.2, and 4.3.

Algorithm	Threshold ₂	POD	TSS	HSS	SEDS	SEDI
SFIP _{mod}	0.3	0.75	0.066	0.047	0.042	0.101
SFIPPT	0.5	0.5	0.184	0.172	0.157	0.265
SFIP	0.35	0.25	0.092	0.103	0.115	0.156

Figure 4.19 indicates that if the threshold₁ decreases from 0.2 to 0.1, the SFIP_{mod} algorithm still presents the highest POD score, when compared with the other algorithms. Besides, the POD of both

the SFIP_{mod} and SFIPPT algorithms increases with this decrease of the threshold₁, while the POD of the SFIP algorithm remains the same. With the new threshold₁ the SFIP_{mod} algorithm forecasts 87.5% of the severe icing events, and SFIPPT forecasts 62.5% of the observed events. The contingency tables relative to the new value of threshold₁ can be found in Appendix A (Tables A.2, A.3 and A.4).

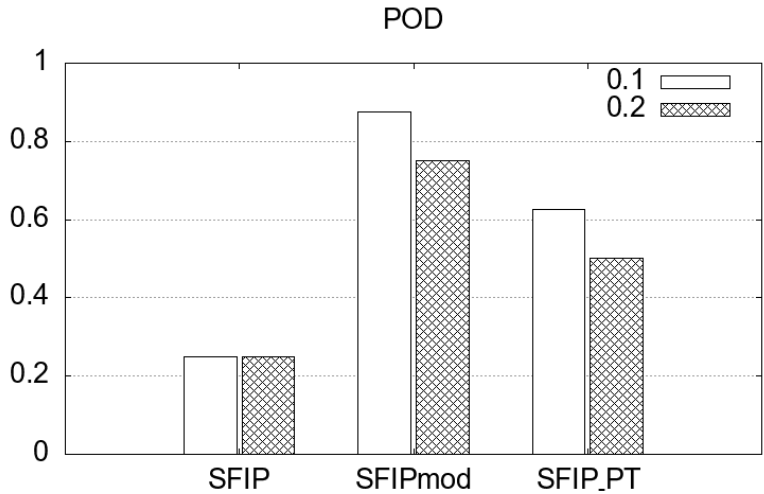


Figure 4.19: POD score for the three algorithms for two different values of threshold₁: 0.1 and 0.2. The values displayed are based on the values of threshold₂ that maximize TSS for each algorithm.

In terms of TSS, Figure 4.20 indicates that this score also increases with the same decrease of the threshold₁ for both the SFIP_{mod} and SFIPPT algorithms, because in both cases the number of correct forecasts increases (see Tables A.2 and A.3). Concerning the SFIP algorithm, the TSS remains the same despite the change in threshold₁, since the contingency table is the same for both cases (see Table A.4). Comparing the results of TSS with Figure 7 (b) from Belo-Pereira [13], the values attained in the present study are considerably low when compared to the TSS values attained in a study with a much larger sample of icing events.

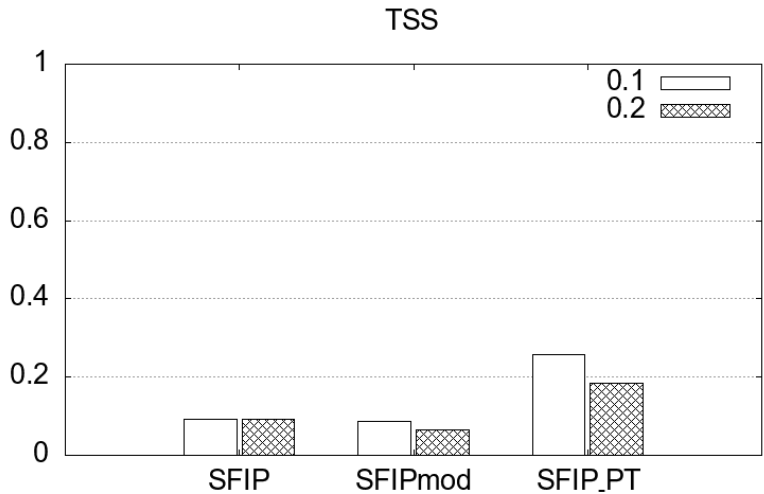


Figure 4.20: TSS score for the three algorithms for two different values of threshold₁: 0.1 and 0.2. The values displayed are based on the values of threshold₂ that maximize TSS for each algorithm.

The HSS score has a similar behaviour to the TSS, as illustrated in Figure 4.21.

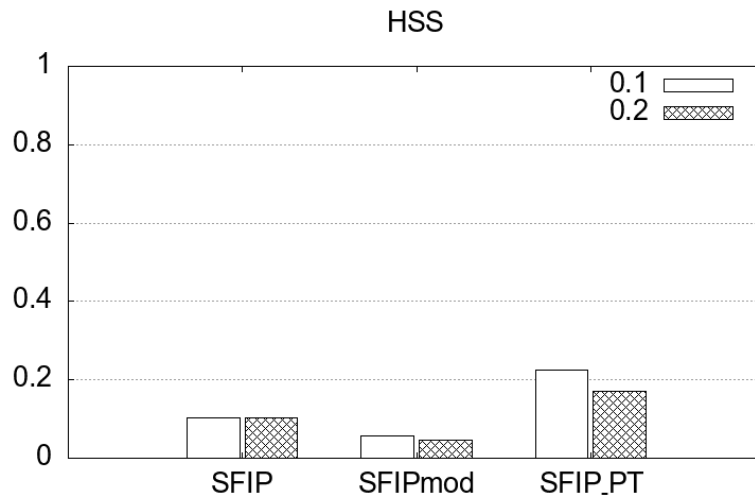


Figure 4.21: HSS score for the three algorithms for two different values of threshold₁: 0.1 and 0.2. The values displayed are based on the values of threshold₂ that maximize TSS for each algorithm.

Figure 4.22 indicates that the SEDS score increases with the change of threshold₁ from 0.2 to 0.1. However, this score increases slightly less than the TSS and HSS. This is due to the fact that, the SEDS score is less influenced by the increase in false alarms because it is harder to hedge¹ than the TSS and HSS.

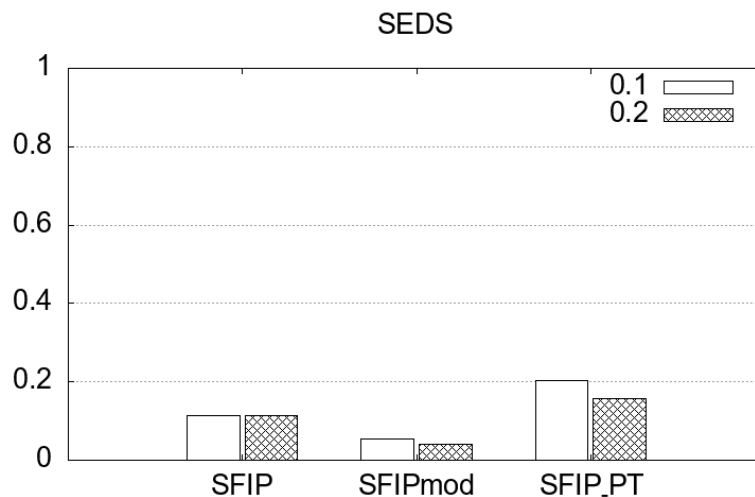


Figure 4.22: SEDS score for the three algorithms for two different values of threshold₁: 0.1 and 0.2. The values displayed are based on the values of threshold₂ that maximize TSS for each algorithm.

Figure 4.23 shows that the SEDI score also increases when the threshold₁ decreases from 0.2 to 0.1. Given that this score is hard to hedge and base rate independent (Ferro and Stephenson [36]), this increase in the score is solely due to the increase of the number of hits for this alteration of the threshold₁ value.

¹ **Hedging.** Act of increasing a score by increasing the number of false alarms

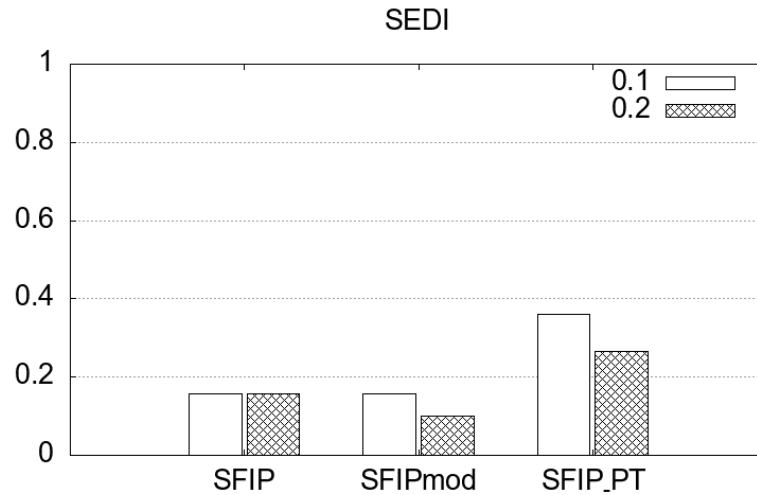


Figure 4.23: SEDI score for the three algorithms for two different values of threshold₁: 0.1 and 0.2. The values displayed are based on the values of threshold₂ that maximize TSS for each algorithm.

After the discussion presented, it is clear that the SFIPPT algorithm outperforms the other two algorithms in the task of distinguishing between severe icing and moderate icing events. The SFIP_{mod} has the poorest performance. However, the sample is very small and this comparison should be performed for a larger sample. Moreover, the maximum TSS is slightly lower than those found by Belo-Pereira [13].

Chapter 5

Conclusions

Aircraft in-flight icing is defined as ice accretion on the airframe during flight. Ice accretion or ice accumulation occurs in the presence of liquid water droplets at sub-freezing temperatures (known as supercooled droplets). As it was made clear, aircraft icing poses a great threat to aviation in general. Ice accumulation on aircraft surfaces, specially wings and tail, can lead to a decrease of lift, increase of drag, loss of control effectiveness and overall performance degradation. This is why the development and improvement of algorithms capable of forecasting icing conditions are of great importance. The main goal of this dissertation was to increase the knowledge about the environments favourable to aircraft icing in the Western European region. For this purpose, PIREPs of icing events and forecasts from one NWP model were analyzed.

In this dissertation, an algorithm to infer aircraft icing was built based on the algorithms implemented in Portugal, by IPMA, and later in the United Kingdom, by the Met Office. For this purpose, a database consisting of 27 reports of icing (moderate or severe) and the NWP forecasts of atmospheric variables such as temperature, relative humidity, vertical velocity and others was gathered. These events were reported over western Europe (Iberian Peninsula, the Balearic Sea, the United Kingdom, Ireland, and the Azores), with 19 events of moderate icing and 8 of severe icing. Most of the reported icing events took place during wintertime, which was expected since atmospheric conditions conducive to icing are more common during winter months. Moreover, in general, the severe icing events occur in a thin layer (thickness inferior to 1000 ft) whereas most of the moderate events (approximately 74%) occurred for a thickness varying between 1000 ft and 10000 ft, with a more expressive percentage between 1000 and 2000 ft.

After analyzing the data from observations, forecasts from the ECMWF deterministic model for the dates and locations of each reported icing event were also analyzed. It was found that the majority of the moderate icing events took place at temperatures between -20°C and 0°C , and nearly 70% of the severe icing events occurred at temperatures between -24°C and -8°C . Moreover, approximately 44% of severe icing events were reported at temperatures below -20°C . In terms of CLWC, most of the severe

and moderate events occurred for values higher than 0.0005 g/kg. A small percentage of moderate events took place for values higher than 0.2 g/kg, while none of the severe events occurred above this value. The forecasts of relative humidity showed that the vast majority of severe and moderate events occurred for values greater than 80%. Concerning TCC, the model data showed more than half (about 58%) of the moderate icing events happened for TCC higher than 0.01 g/kg and around 81% of the severe events occurred beyond the 0.0005 g/kg threshold.

A new quantity was also determined using the forecasts: the icing layer of CLWC or RH exceeding a certain threshold. The maximum thickness between these two layers was selected for each event. The distribution of this quantity showed that the majority (over 60%) of both severe and moderate icing events occurred for a thickness between 50 hft and 100 hft. This suggests that this quantity could be a useful predictor of the conditions conducive to icing events.

The results aforementioned were important to adjust the thresholds of the membership functions used in the new algorithm, and to create the new membership function of TCC. The membership functions of the new index were compared with the membership functions of the IPMA algorithm. Overall, the functions from both algorithms were similar with the exception of the CLWC function. Since most of icing events occurred for low CLWC, the new function gives more weight to these low values of CLWC (when compared with the IPMA membership function).

The three algorithms were computed for all the events reported using the forecasts from the ECMWF model. The behaviour of these algorithms was analyzed in detail for four different icing events (two moderate and two severe). These examples showed that the new algorithm tends to forecast icing layers with greater thickness than the layers forecast by the other two algorithms. This reflects the influence of the membership function of temperature. Moreover, the vast majority of the layers predicted by the Met Office index have thicknesses inferior to 10 hft.

The performance of the icing algorithms was also assessed using contingency tables and the respective scores. These tables were built for different thresholds using a series of criteria, which were presented and explained with practical examples. These scores show that the algorithm implemented by IPMA has the best performance concerning the ability to distinguish between severe icing and moderate icing events, while the new algorithm reveals the poorest performance. However, this result may be influenced by the fact that, the database used was small. In a near future, this comparison should be performed for a larger sample.

As a final remark, it is important to note that the task of forecasting the icing severity, in particular, of distinguishing severe from moderate icing is considerably challenging, as suggested by various studies. For example, the study conducted by Belo-Pereira [13] in 2015, showed that all the algorithms considered in the study had a better performance in forecasting the icing occurrence than its severity. Another study made by Kalinka et al. [25] in 2017 relative to an icing warning system for European airspace

showed that, despite the improvements in the overall skill of the system, there was still considerable room for improvement concerning the prediction of the icing severity. Fowler et al. [42] drew similar conclusions relative to the CIP algorithm. Moreover, they suggested that this shortcoming could be related in some extent to the biased and subjective nature of PIREPs. Combining this with the sample size, it was expected that the scores attained in this study would be lower than those obtained in studies with larger samples, and that only aimed at forecasting the icing occurrence rather than icing severity.

5.1 Future Work

In the future, it would be interesting to evaluate the impact of using a much larger database. In addition, it would be interesting to study the impact on short-term forecasts of integrating satellite and radar observations, as this information allows for a more complete characterization of the icing environments.

Another path worth exploring is the introduction of a membership function of the CLWC or RH maximum thickness mentioned above, since the distribution of this quantity suggested that this could be a useful predictor of the icing potential.

Lastly, the database used does not include PIREPs of negative icing conditions, i.e., PIREPs relative to the non-occurrence of icing. This information is important to quantify the over-forecasting and, consequently, the false alarm-rates. As it was discussed, false alarms dominated the contingency tables of the new index. However, negative icing conditions are not provided in sufficient quality by the PIREPs (Kalinka et al. [25]).

Bibliography

- [1] J. Mazon, J. I. Rojas, M. Lozano, D. Pino, X. Prats, and M. M. Miglietta. Influence of meteorological phenomena on worldwide aircraft accidents, 1967–2010. *Meteorological Applications*, 25:236–245, 4 2018. ISSN 14698080. doi: 10.1002/met.1686.
- [2] Annex 3 to the Convention on International Civil Aviation. In *Meteorological Service for International Air Navigation, 20th edn.*, page 224, Montreal, Canada, 2018. International Civil Aviation Organization (ICAO).
- [3] R. L. Bowyer and P. G. Gill. Objective verification of global in-flight icing forecasts using satellite observations: Verification of WAFS icing forecasts using satellite observations. *Meteorological Applications*, 26:610–619, 10 2019. ISSN 14698080. doi: 10.1002/met.1788.
- [4] W. R. Sand, W. A. Cooper, M. K. Politovich, and D. L. Veal. Icing Conditions Encountered by a Research Aircraft. *Journal of Applied Meteorology and Climatology*, 23:1427–1440, 10 1984. doi: <https://doi.org/10.1175/0733-3021-23.10.1427>.
- [5] P. Schultz and M. K. Politovich. Toward the Improvement of Aircraft-Icing Forecasts for the Continental United States. *Weather and Forecasting*, 7:491–500, 9 1992.
- [6] D. Rosenfeld and W. L. Woodley. Deep convective clouds with sustained supercooled liquid water down to -37.5°C. *Nature*, 405:440–442, 5 2000. doi: <https://doi.org/10.1038/35013030>.
- [7] K. Petty and C. Floyd. A Statistical Review of Aviation Airframe Icing Accidents in the U.S. 10 2004.
- [8] S. D. Green. A Study of U. S. Inflight Icing Accidents and Incidents, 1978 to 2002, 1 2006.
- [9] G. Dillingham. Aviation Safety: Preliminary Information on Aircraft Icing and Winter Operations. In *Testimony Before the Subcommittee on Aviation, Committee on Transportation and Infrastructure, House of Representatives*, Washington, D.C., 2010. United States Government Accountability Office.
- [10] G. Thompson, R. T. Brientjes, B. G. Brown, and F. Hage. Intercomparison of In-Flight Icing Algorithms. Part I: WISP94 Real-Time Icing Prediction and Evaluation Program. *Weather and Forecasting*, 12:878–889, 12 1997.
- [11] B. C. Bernstein, F. Mcdonough, M. K. Politovich, B. G. Brown, T. P. Ratvasky, D. R. Miller, C. A. Wolff, and G. Cuning. Current Icing Potential: Algorithm Description and Comparison with Aircraft

- Observations. *Journal of Applied Meteorology and Climatology*, 44:969–986, 7 2005. URL <http://adds.aviationweather.gov>.
- [12] F. McDonough, B. C. Bernstein, M. K. Politovich, and C. A. Wolff. The Forecast Icing Potential (FIP) Algorithm. pages 231–238. American Meteorological Society, 1 2004.
- [13] M. Belo-Pereira. Comparison of in-flight aircraft icing algorithms based on ECMWF forecasts. *Meteorological Applications*, 22:705–715, 10 2015. ISSN 14698080. doi: 10.1002/met.1505.
- [14] C. Morcrette, K. Brown, R. Bowyer, P. Gill, and D. Suri. Development and Evaluation of In-Flight Icing Index Forecast for Aviation. *Weather and Forecasting*, 34:731–750, 6 2019. ISSN 0882-8156. doi: 10.1175/WAF-D-18-0177.1. URL <https://journals.ametsoc.org/doi/10.1175/WAF-D-18-0177.1>.
- [15] S. G. Cober, J. W. Starpp, and G. A. Isaac. An Example of Supercooled Drizzle Drops Formed through a Collision-Coalescence Process. *Journal of Applied Meteorology*, 35:2250–2260, 12 1996. doi: [https://doi.org/10.1175/1520-0450\(1996\)035%3C2250:AEOSDD%3E2.0.CO;2](https://doi.org/10.1175/1520-0450(1996)035%3C2250:AEOSDD%3E2.0.CO;2).
- [16] H. A. J. and L. M. Miloshevich. Homogeneous Ice Nucleation and Supercooled Liquid Water in Orographic Wave Clouds. *Journal of Atmospheric Sciences*, 50:2335–2353, 8 1993. doi: [https://doi.org/10.1175/1520-0469\(1993\)050%3C2335:HINASL%3E2.0.CO;2](https://doi.org/10.1175/1520-0469(1993)050%3C2335:HINASL%3E2.0.CO;2).
- [17] G. Isaac and R. Schemenauer. Large Particles in Supercooled Regions of Northern Canadian Cumulus Clouds. *Journal of Applied Meteorology*, 18:1056–1065, 8 1979. doi: [https://doi.org/10.1175/1520-0450\(1979\)018%3C1056:LPISRO%3E2.0.CO;2](https://doi.org/10.1175/1520-0450(1979)018%3C1056:LPISRO%3E2.0.CO;2).
- [18] Y. Hu, S. Rodier, K. M. Xu, W. Sun, J. Huang, B. Lin, P. Zhai, and D. Josset. Occurrence, liquid water content, and fraction of supercooled water clouds from combined CALIOP/IIR/MODIS measurements. *Journal of Geophysical Research Atmospheres*, 115, 2010. ISSN 01480227. doi: 10.1029/2009JD012384.
- [19] R. M. Rauber and A. Tokay. An Explanation for the Existence of Supercooled Water at the Top of Cold Clouds. *Journal of Atmospheric Sciences*, 48:1005–1023, 4 1991.
- [20] W. A. Cooper and G. Vali. The Origin of Ice in Mountain Cap Clouds. *Journal of the Atmospheric Sciences*, 38:1244–1259, 6 1981. doi: [https://doi.org/10.1175/1520-0469\(1981\)038%3C1244:TOOIM%3E2.0.CO;2](https://doi.org/10.1175/1520-0469(1981)038%3C1244:TOOIM%3E2.0.CO;2).
- [21] R. J. Hansman. Droplet Size Distribution Effects on Aircraft Ice Accretion. *Journal of Aircraft*, 22: 503–508, 6 1985. ISSN 00218669. doi: 10.2514/3.45156.
- [22] Y. Cao, Z. Wu, Y. Su, and Z. Xu. Aircraft flight characteristics in icing conditions. *Progress in Aerospace Sciences*, 74:62–80, 4 2015. ISSN 03760421. doi: 10.1016/j.paerosci.2014.12.001.
- [23] M. K. Politovich. Response of a Research Aircraft to Icing and Evaluation of Severity Indices. *Journal of Aircraft*, 33:291–297, 3 1996. ISSN 0021-8669. doi: 10.2514/3.46936.

- [24] C. Gencer, E. K. Aydogan, and Çetin Karahan. An Algorithm Predicting Upper Level Icing Potential by Fuzzy Set Theory and an Application with this Algorithm for Turkey. *The Open Industrial & Manufacturing Engineering Journal*, 3:7–12, 2010.
- [25] F. Kalinka, K. Roloff, J. Tendel, and T. Hauf. The In-flight icing warning system ADWICE for European airspace - Current structure, recent improvements and verification results. *Meteorologische Zeitschrift*, 26:441–455, 2017. ISSN 16101227. doi: 10.1127/metz/2017/0756.
- [26] F. Boudala, G. A. Isaac, and D. Wu. Aircraft Icing Study Using Integrated Observations and Model Data. *Weather and Forecasting*, 34:485–506, 6 2019. ISSN 15200434. doi: 10.1175/WAF-D-18-0037.1.
- [27] G. Thompson. High Resolution Numerical Weather Model Forecasts of Icing at the Ground and in the Air. 2019.
- [28] W. C. Skamarock and J. B. Klemp. A time-split nonhydrostatic atmospheric model for weather research and forecasting applications. *Journal of Computational Physics*, 227:3465–3485, 3 2008. ISSN 0021-9991. doi: 10.1016/J.JCP.2007.01.037.
- [29] B. Schwartz. The quantitative use of pireps in developing aviation weather guidance products. *Weather and Forecasting*, 11:372–384, 9 1996. doi: [https://doi.org/10.1175/1520-0434\(1996\)011\%3C0372:TQUOPI\%3E2.0.CO;2](https://doi.org/10.1175/1520-0434(1996)011\%3C0372:TQUOPI\%3E2.0.CO;2).
- [30] Portal do Clima. Monthly Average Temperature in Portuguese Territory. <http://portaldoclima.pt/pt/>. Accessed: 09/03/2022.
- [31] S. Malardel, C. Kühnlein, N. Wedi, W. Deconinck, M. Diamantakis, M. George, M. Hamrud, and P. K. Smolarkiewicz. A new grid for the IFS. *ECMWF Newsletter*, 146:23–28, 1 2016. URL <https://www.researchgate.net/publication/297695132>.
- [32] J. K. Williams. Introduction to Fuzzy Logic. In S. E. Haupt, A. Pasini, and C. Marzban, editors, *Artificial Intelligence Methods in Environmental Sciences*, chapter 6, pages 127–151. Springer, 2009.
- [33] J. E. Thornes and D. B. Stephenson. How to judge the quality and value of weather forecast products. *Meteorological Applications*, 8:307–314, 2001. ISSN 13504827. doi: 10.1017/S1350482701003061.
- [34] S. Gold, E. White, W. Roeder, M. McAleenan, C. S. Kabban, and D. Ahner. Probabilistic Contingency Tables: An Improvement to Verify Probability Forecasts. *Weather and Forecasting*, 35: 609–621, 4 2020. ISSN 15200434. doi: 10.1175/WAF-D-19-0116.1.
- [35] C. A. D. III, R. Davies-Jones, and D. L. Keller. On Summary Measures of Skill in Rare Event Forecasting Based on Contingency Tables. *Weather and Forecasting*, 5:576–585, 1990.

- [36] C. A. Ferro and D. B. Stephenson. Extremal Dependence Indices: Improved Verification Measures for Deterministic Forecasts of Rare Binary Events. *Weather and Forecasting*, 26:699–713, 10 2011. ISSN 08828156. doi: 10.1175/WAF-D-10-05030.1.
- [37] M. Belo-Pereira. Aviation Turbulence Forecasting over the Portuguese Flight Information Regions: Algorithm and Objective Verification. *Atmosphere*, 13, 3 2022. ISSN 20734433. doi: 10.3390/atmos13030422.
- [38] R. J. Hogan, E. J. O’Connor, and A. J. Illingworth. Verification of cloud-fraction forecasts. *Quarterly Journal of the Royal Meteorological Society*, 135:1494–1511, 7 2009. ISSN 00359009. doi: 10.1002/qj.481.
- [39] D. B. Stephenson, B. Casati, C. A. Ferro, and C. A. Wilson. The extreme dependency score: a non-vanishing measure for forecasts of rare events. volume 15, pages 41–50. John Wiley and Sons Ltd, 2008. doi: 10.1002/met.53.
- [40] A. Korolev, G. McFarquhar, P. R. Field, C. Franklin, P. Lawson, Z. Wang, E. Williams, S. J. Abel, D. Axisa, S. Borrmann, J. Crosier, J. Fugal, M. Krämer, U. Lohmann, O. Schenczek, M. Schnaiter, and M. Wendisch. Mixed-Phase Clouds: Progress and Challenges. *Meteorological Monographs*, 58:5.1–5.50, 1 2017. ISSN 0065-9401. doi: 10.1175/amsmonographs-d-17-0001.1.
- [41] J. Marwitz, M. Poiitovich, B. Bernstein, F. Ralph, P. Neiman, R. Ashenden, and J. Bresch. Meteorological Conditions Associated with the ATR72 Aircraft Accident near Roselawn, Indiana, on 31 October 1994. *Bulletin of the American Meteorological Society*, 78:41–52, 1 1997. doi: [https://doi.org/10.1175/1520-0477\(1997\)078\%3C0041:MCAWTA\%3E2.0.CO;2](https://doi.org/10.1175/1520-0477(1997)078\%3C0041:MCAWTA\%3E2.0.CO;2).
- [42] T. L. Fowler, M. Chapman, B. G. Brown, and J. L. Mahoney. Quality Assessment Report: CURRENT ICING POTENTIAL (CIP) SEVERITY INDEX, 2004.

Appendix A

Supporting Figures and Tables

Figure A.1 shows the distribution of the maximum Vertical Velocity in the troposphere, in Pa s^{-1} . Unlike Figure 4.5, positive values represent downward motion and negative values correspond to upward motion. The values of Vertical Velocity in Pa s^{-1} were used to compute the vertical velocity membership function of the SFIPPT algorithm.

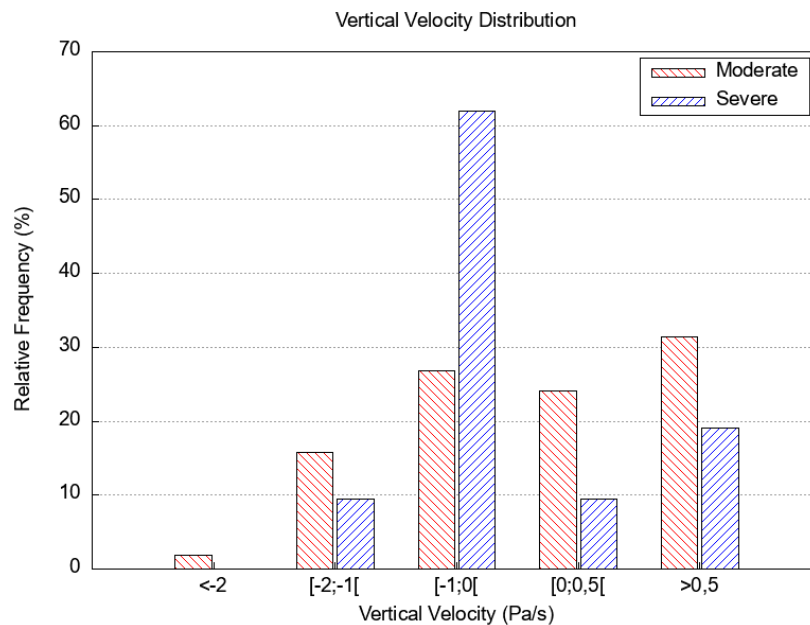


Figure A.1: Vertical Velocity relative frequency distribution

Table A.1 shows information about the forecasts made by each algorithm with the data of each icing event in the database. More specifically, it shows the number of icing layers forecast by each algorithm for all the reported icing events and the location of the reported layer relative to the forecast layer(s). In the case of the forecast layer not intercepting the observed layer, the second column of "Location" indicates the distance between those two layers (in hft).

Table A.1: Layer forecast for each algorithm

Event No.	SFIP		SFIP _{mod}		SFIPPT				
	Layers	Location	Layers	Location	Layers	Location			
1	0	-	-	1	1 st layer	upper half	1	1 st layer	upper half
2	1	1 st layer	upper half	1	1 st layer	upper half	1	1 st layer	upper half
3	0	-	-	1	1 st layer	upper half	1	1 st layer	upper half
4	0	-	-	2	2 nd layer	upper half	2	2 nd layer	upper half
5	0	-	-	1	1 st layer	lower half	2	1 st layer	all
6	0	-	-	1	1 st layer	82.185	1	1 st layer	41.784
7	1	1 st layer	lower half	1	1 st layer	middle	1	1 st layer	middle
8	0	-	-	1	1 st layer	upper half	1	1 st layer	upper half
9	0	-	-	1	1 st layer	upper half	1	1 st layer	37.429
10	1	1 st layer	upper half	1	1 st layer	upper half	1	1 st layer	upper half
11	0	-	-	1	1 st layer	all	1	1 st layer	all
12	1	1 st layer	all	1	1 st layer	upper half	1	1 st layer	upper half
13	0	-	-	1	1 st layer	71.929	0	-	-
14	0	-	-	1	1 st layer	upper half	2	1 st layer	all
15	0	-	-	1	1 st layer	upper half	2	2 nd layer	all
16	0	-	-	1	1 st layer	upper half	1	1 st layer	middle
17	0	-	-	1	1 st layer	middle	1	1 st layer	middle
18	0	-	-	1	1 st layer	4.003	1	1 st layer	4.003
19	1	1 st layer	44.89	1	1 st layer	lower half	2	1 st layer	lower half
20	1	1 st layer	34.225	1	1 st layer	5.981	1	1 st layer	5.981
21	0	-	-	2	2 nd layer	12,112	1	1 st layer	21.611
22	0	-	-	1	1 st layer	3,232	1	1 st layer	3.232
23	1	1 st layer	11.133	1	1 st layer	upper half	1	1 st layer	upper half
24	1	1 st layer	52.958	1	1 st layer	14.188	1	1 st layer	38.268
25	0	-	-	0	-	-	1	1 st layer	74.752
26	1	1 st layer	upper half	1	1 st layer	upper half	1	1 st layer	upper half
27	0	-	-	2	2 nd layer	lower half	2	2 nd layer	lower half

Tables A.2, A.3 and A.4 are the contingency tables relative to the discussion made about the scores in Section 4.4. The scores attained with these tables are shown in the histograms from Figure 4.19 to Figure 4.23.

Table A.2: Contingency Table of SFIP_{mod} algorithm forecasts for a threshold₁ of 0.1 and a threshold₂ of 0.1.

Forecast	Observation	
	Yes	No
Yes	7	15
No	1	4

Table A.3: Contingency Table of SFIPPT algorithm forecasts for a threshold₁ of 0.1 and a threshold₂ of 0.5.

Forecast	Observation	
	Yes	No
Yes	5	7
No	3	12

Table A.4: Contingency Table of SFIP algorithm forecasts for a threshold₁ of 0.1 and a threshold₂ of 0.35.

Forecast	Observation	
	Yes	No
Yes	2	3
No	6	16

